*Physics – Uspekhi* **64** (4) 325 – 343 (2021) 

*REVIEWS OF TOPICAL PROBLEMS* PACS numbers: 21.10.Dr, 21.10.Re

# Phase transitions in atomic nuclei

R V Jolos, E A Kolganova

DOI: https://doi.org/10.3367/UFNe.2020.06.038787

## Contents



**Abstract. Numerous examples show phase transitions in the structure of atomic nuclei as the excitation energy and the moment of rotation increase and the number of nucleons changes. These are phase transitions of the equilibrium shape and structure of the ground and low-lying excited states of the nuclei, associated with a change in their symmetry. The subject of phase transitions has given rise to a new wave of investigations into the structure of atomic nuclei. In this review, we consider examples of phase transitions, discuss the feasibility of describing them within a collective model of the nucleus with a Hamiltonian depending on a small number of dynamic variables, and also touch upon microscopic aspects of phase transitions.**

**Keywords:** nuclear physics, phase transitions, nucleus structure, nucleus shape, deformation, collective excitations

## 1. Introduction

The subject of this review is mainly heavy atomic nuclei, with the number of nucleons $A$ greater than 100, although abundant examples of quantum phase transitions are also provided by lighter nuclei. Heavy atomic nuclei are systems with a huge number of degrees of freedom, namely, $3(A-1)$. Quite remarkably, under moderate excitation energies, e.g., in the range of 1–2 MeV for heavy nuclei, their properties can be described based on a Hamiltonian with only a small number of dynamical variables. For example, the most important dynamical variable that determines the properties of nuclei at small excitation energies is the quadrupole mode [1, 2], which includes five degrees of freedom, by the number of the angular momentum projections. Certainly, these five degrees of freedom are related in a most intricate way to the coordinates describing the motion of individual nucleons (the random phase approximation, the generator coordinate method, bosonic expansions, the model of interacting bosons, etc. [3]), but in a phenomenological analysis the Hamiltonian contains only these dynamical variables. Describing excited states of the nuclei associated with rotations and quadrupole oscillations of the equilibrium shape, such a Hamiltonian also accounts for their effect on the motion of individual nucleons.

Some other dynamical variables, in addition to the quadrupole mode, can also be called collective variables because of their relation to changes in the state of motion of a large number of nucleons. They are the dynamical variables describing octupole shape oscillations [4], pair correlations of nucleons [5, 6], fluctuations of the angular momentum direction of the deformed nucleus with respect to the axial symmetry axis [7], and chirality in odd–odd nuclei [8].

The collective variables related to the quadrupole and octupole degrees of freedom are directly related to the notion of equilibrium shape of an atomic nucleus, primarily in the ground state. This gave rise to the notions of spherical, deformed, and transitional nuclei, the last of which occupy an intermediate position between spherical and deformed. Studies of the structure of nuclei, mostly with the use of Coulomb excitation, have shown that the nucleus shape in the

**R V Jolos** (†), **E A Kolganova** (‡)
Joint Institute for Nuclear Research,
ul. Joliot-Curie 6, 141980 Dubna, Moscow region, Russian Federation;
Dubna State University,
ul. Universitetskaya 19, 141980 Dubna, Moscow region,
Russian Federation
E-mail: (†) jolos@theor.jinr.ru, (‡) kea@theor.jinr.ru

Received 12 April 2020, revised 12 June 2020
*Uspekhi Fizicheskikh Nauk* **191** (4) 337 – 357 (2021)
Translated by S Alekseev

ground state depends on the proton–neutron content of the nucleus and changes with the number of protons and neutrons. This has led to the notion of phase transitions from spherical nuclei to deformed nuclei as the number of nucleons changes. Surely, these are not quite the phase transitions well known from thermodynamics, which occur as the temperature and pressure vary. Due to the finite number of nucleons in a nucleus, these transition from one shape to another are smeared (although sharp changes in shape are also observed under insignificant changes in the number of nucleons). It must also be kept in mind that the number of nucleons, being a discrete parameter, cannot serve as a rigorously defined control parameter. Strictly speaking, the signatures and indications of the quantum phase transition observed in nuclei are arguably 'precursors' of real phase transitions that could have occurred in nuclei if they had been infinite in volume. At the same time, calculations allow us to use continuous variations in control parameters, thus making the 'precursor' of phase transitions more pronounced.

In considering stable nuclei, phase transitions have been observed under a variation in not only the number of nucleons but also the angular momentum of the nucleus. In recent years, the interest of nuclear physicists has shifted toward investigations of nuclei far from the stability domain. In such nuclei, at different excitation energies, states have been discovered in which the nucleus takes entirely different shapes. This has given rise to the concept of coexistence of shapes [9–11].

## 2. Deformation generation mechanism

A fundamental feature of an atomic nucleus, setting it apart from many other microsystems, is the self-consistent field formed as a result of the collective motion of a large number of nucleons. A characteristic feature of the self-consistent field of the nucleus is the presence of nuclear shells, the shell structure [12]. Studies of the structure of atomic nuclei began with attempts to explain the origin of magic numbers of protons and neutrons, i.e., the numbers making the nucleus especially stable. The explanation has been found: the shell structure of the nuclei and the existence of an energy gap separating the shells. Another finding was that all magic nuclei are spherical. The situation started to change when experimental investigations of nuclei far from the stability domain became feasible.

We consider the mechanism of the occurrence of deformations in a nucleus within an approach relying on the notion of the mean field of the nucleus and of nucleons moving in that field. In this setting, the deformation occurs as a result of the polarization of the nucleus core by valence nucleons filling certain orbits. The relation between valence nucleons and oscillations of the nucleus core leads to the nuclear Jahn–Teller effect [13], i.e., to instability of the spherical symmetry of the mean field under deformations that reduce that symmetry. The fact that an atomic nucleus is not necessarily spherical was first noted back in 1936 by Niels Bohr in [14], where he formulated the main principles of the compound nucleus model. A model where the relation between nucleus surface oscillations and the motion of individual nucleons is taken into account was formulated by Aage Bohr in 1952 [1].

The shell model of a nucleus contains two main elements of the mechanism that leads to a reduction in the mean field symmetry of the nucleus: the density of single particle levels as a function of the occupancy of shells and the coupling of the motion of nucleons to oscillations of the core. The possibility itself of separating the nucleus into a core and several valence nucleons interacting via two-particle forces is inherent in the shell model. The stability of one atomic nucleus shape or another is directly related to the density of single particle levels near the Fermi surface. Variations in the density of single particle levels as the shells are being gradually filled have been given an excellent interpretation in terms of periodic orbits of a suitable classical Hamiltonian [15]. In the approach based on the shell model of the nucleus, deformation is related to the appearance of an energy gap in the neutron and proton spectra of single particle levels [16, 17].

The distance between single particle levels in a shell and their relative positions depends on the interaction of valence nucleons and can change as the shell is being filled. The microscopic mechanism underlying phase transitions from spherical to deformed nuclei is the Federman–Pittel mechanism [18], the key role in which is played by the monopole proton–neutron interaction [19–21] of the nucleons filling the single particle orbit with a strong spatial overlap. The point is that the structure of nuclear shells and their content (the single particle levels they are made of) depend on the proton–neutron content of the nucleus. The interaction of nucleons, due to its specific dependence on the orientation of spins and isospins, can in some cases substantially change the distance between single particle levels. This gives rise to new shells, i.e., a new magic number, and new subshells, i.e., gaps between single particle levels in one shell. Such examples were first given by Cohen [22] in 1968 at a Dubna symposium on the structure of atomic nuclei. An example is provided by the interaction of protons in the $1g_{9/2}$ state with neutrons in the $1g_{7/2}$ state.

Later, in the work by Otsuka and his group [23], it was shown that just the tensor interaction of nucleons is responsible for the observed effects. Tensor interaction can essentially change the position of single particle levels in a shell not only when the proton–neutron content of the nucleus changes but also during excitation of the nucleus, when particle–hole excitations lead to a change in the filling of single particle levels by valence nucleons. The new subshells can then have characteristics different from those inherent in the ground state. For example, they can be orbits with a large orbital momentum, which are therefore also characterized by high quadrupole momenta. Such excited configurations exhibit larger distortions, i.e., have a shape different from the nucleus shape in the ground state. As a result, phase transitions from the spherical to a distorted shape of the nucleus become possible as the excitation energy increases.

The leading role in the generation of distortions of the nucleus is thus played by proton–neutron interaction in the channel with the isospin $T = 0$ [24], whereas the interaction with $T = 1$ can be associated with short-range pair forces stabilizing the spherical shape of the nucleus [25–28]. For example, semimagic nuclei, which have only one type of valence nucleon, either protons or neutrons, are spherical. Instructive examples are provided by the spherical nucleus $^{20}$O with four valence neutrons and the deformed nucleus $^{20}$Ne with two valence protons and two valence neutrons.

## 3. Collective model of the nucleus

An atomic nucleus is a fully quantum system whose Hamiltonian has rotation invariance. This means that the

nucleus has no preferred direction in space. But in that case, it is difficult to determine the shape of the nucleus. Indeed, the nucleus shape is not observable. To introduce nucleus shape into consideration, we must break the rotation invariance, i.e., define an internal coordinate system rigidly attached to the nucleus. In addition, we must introduce a semiclassical model similar to that of a liquid drop in order to define the parameters characterizing the shape of the nucleus [1]. The problem then arises of how to identify suitable parameters using the wave function of the nucleus defined in the laboratory coordinate system.

Historically, however, the course of investigations took a different path. In 1953, A Bohr and B Mottelson [29] related the appearance of rotational bands in excitation spectra of nuclei to their deformation in the internal coordinate system. Since then, shapes of the nuclei have been discussed based on the notion of the mean field of the nucleus defined in the internal coordinate system. The deformation parameters are then given by components of the quadrupole moment of the nucleus density, defined in the internal coordinate system. From the quadrupole moment defined in the internal coordinate system, we can move to the quadrupole moment defined in the laboratory system. Using quadrupole moment components and canonically conjugate momenta as dynamical variables, we can construct a rotation-invariant Hamiltonian in the laboratory system. This led to the geometric collective model of the nucleus with A Bohr's Hamiltonian [1].

Distortions of the nuclei and their shapes were also discussed within algebraic collective models based on one dynamical symmetry group or another. The first such model, proposed by Elliott [30, 31], went practically unnoticed, however, partly because of its limited applicability range. Popularity was gained by the algebraic collective model based on the SU(6) dynamical symmetry group [32, 33].

### 3.1 Geometric collective model

The geometric collective model was formulated by A Bohr as a hydrodynamic collective model deriving from the already existing liquid-drop model of the nucleus [34, 35]. However, many of these early notions turned out to be too restrictive and were in fact not necessary. In the final formulation, the collective variables were chosen as the multipole moments of the nucleus density. This was convenient also because microscopic expressions for them are known in terms of nucleon coordinates. Among such moments, the main role is played by the quadrupole moment of nucleus density. The corresponding collective coordinates are the five components of the quadrupole tensor $\alpha_{2\mu}$, proportional to the quadrupole moment of the nucleus. In order to consider rotational excitations of the nuclei and excitation due to nucleus shape oscillations, it is convenient to separate dynamical variables associated with rotational degrees of freedom and the dynamical variables characterizing the nucleus shape:

$$\alpha_{2\mu} = \beta\left[D^2_{\mu 0}(\boldsymbol{\Omega})\cos\gamma + \frac{1}{\sqrt{2}}\left(D^2_{\mu 2}(\boldsymbol{\Omega}) + D^2_{\mu -2}(\boldsymbol{\Omega})\right)\sin\gamma\right]. \quad (1)$$

Here, $D^2_{\mu k}(\boldsymbol{\Omega})$ is the Wigner function depending on the three Euler's angles $\boldsymbol{\Omega}$, which define the orientation of the internal coordinate system of the nucleus with respect to the laboratory system. The variable $\beta$ characterizes the deviation of the nucleus shape from spherical, and nonvanishing values of $\gamma$ imply that the nucleus has no axial symmetry. For example, in the case of axially symmetric quadrupole deformation, with the nucleus shape represented as an ellipsoid of rotation, the ratio of the minor semiaxis of the ellipsoid to the major semiaxis is $[1-(2/3)\beta]/[1+(1/3)\beta]$. Typical values of $\beta$ for deformed nuclei from the range of actinides and rare-earth nuclei are 0.25–0.30.

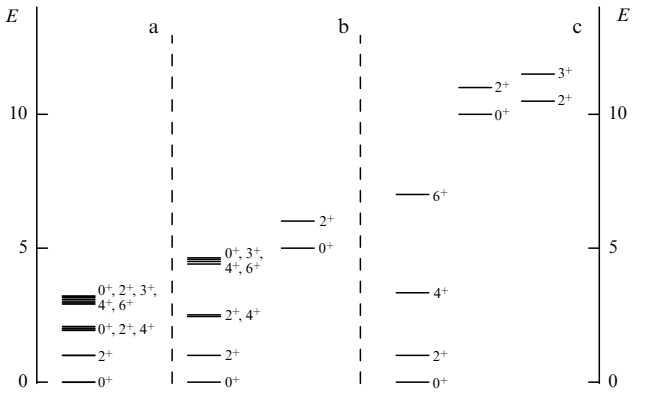


**Figure 1.** Spectra of low-lying collective excited states: (a) five-dimensional harmonic oscillator, (b) soft nonaxial rotor, and (c) axially symmetric rotor.

The collective Hamiltonian of the nucleus in terms of $\beta$, $\gamma$, and $\boldsymbol{\Omega}$ has the form [36]

$$\hat{H} = -\frac{\hbar^2}{2B}\nabla^2 + \hat{V}, \quad (2)$$

where $\hat{V}$ is the potential energy depending only on $\beta$ and $\gamma$, $B$ is the coefficient of inertia, $\nabla^2$ is the Laplacian in five-dimensional space,

$$\nabla^2 = \frac{1}{\beta^4}\frac{\partial}{\partial\beta}\beta^4\frac{\partial}{\partial\beta} - \frac{\hat{\Lambda}^2}{\beta^2}, \quad (3)$$

where

$$\hat{\Lambda}^2 = -\frac{1}{\sin(3\gamma)}\frac{\partial}{\partial\gamma}\sin(3\gamma)\frac{\partial}{\partial\gamma} + \sum_{k=1}^{3}\frac{\hat{L}_k^2}{4\sin^2(\gamma - 2\pi k/3)}, \quad (4)$$

and $\hat{L}_k$ are components of the angular momentum operator. The potential energy $\hat{V}$ is a function of two rotation invariants: $\beta^2$ and $\beta^3\cos(3\gamma)$.

There are three well-known generally accepted models of collective motion in even–even nuclei: vibrator, axially asymmetric rotor, also called the '$\gamma$-soft nucleus,' and an axially symmetric rotor. These three models correspond to three particular cases of collective motion, for which Bohr's Hamiltonian (2) has analytic solutions.

The first model, the vibrator, is obtained by setting $\hat{V} = (1/2)C\beta^2$, where $C$ is the rigidity parameter of the potential. In that case, Bohr's Hamiltonian reduces to the Hamiltonian of the five-dimensional harmonic oscillator with an equidistant spectrum of excited states consisting of degenerate multiplets (Fig. 1a).

The nucleus shape is frequently characterized by the ratio of the excitation energy of the lowest $4^+$ state ($4_1^+$) to the excitation energy of the lowest $2^+$ state ($2_1^+$): $R_{4/2} \equiv E(4_1^+)/E(2_1^+)$. In the case of harmonic oscillations about the spherical shape of the nucleus, $R_{4/2} = 2$.

The next model corresponds to the assumption that the potential $\hat{V}$ is independent of $\gamma$ [37]. Then, the dependence on

$\gamma$ in the Hamiltonian is concentrated only in $\hat{\Lambda}^2$, where $\hat{\Lambda}^2$ is the Casimir operator of the SO(5) group. Its eigenfunctions $\mathcal{Y}_{v\alpha LM}$ and eigenvalues are known [36]:

$$\hat{\Lambda}^2\mathcal{Y}_{v\alpha LM} = v(v+3)\mathcal{Y}_{v\alpha LM}\,, \quad v = 0, 1, 2, \ldots, \tag{5}$$

where $L$ and $M$ are the respective angular momentum and its projection, corresponding to rotation in three-dimensional space, $v$ is the angular momentum quantum number in five-dimensional space (called the Racah seniority), and $\alpha$ is an additional quantum number. In this case, Bohr's Hamiltonian takes the form

$$\left[-\frac{\hbar^2}{2B}\left(\frac{1}{\beta^4}\frac{\partial}{\partial\beta}\beta^4\frac{\partial}{\partial\beta} - \frac{v(v+3)}{\beta^2}\right) + V(\beta)\right]R(\beta) = E_v R(\beta)\,. \tag{6}$$

If we assume that the potential has a deep and narrow minimum at $\beta = \beta_0$, then the spectrum of excited states becomes (Fig. 1b)

$$E_v = \frac{\hbar^2}{2B\beta_0^2}\,v(v+3)\,. \tag{7}$$

Here, $R_{4/2} = 2.5$.

The third model, the axially symmetric rotor, follows from Bohr's Hamiltonian by assuming both $\beta(=\beta_0)$ and $\gamma(=0)$ to be frozen. The spectrum of excited states is then expressed as

$$E_{L,K} = \frac{\hbar^2}{6B\beta_0^2}\left[L(L+1) - K^2\right], \tag{8}$$

where $L$ is the angular momentum and $K$ is the angular momentum projection on the symmetry axis of the nucleus. In this limit, $R_{4/2} = 3.33$. If in the harmonic approximation we also include $\beta$-oscillations about $\beta_0$ and $\gamma$-oscillations about $\gamma = 0$, then the spectrum of excited states becomes (Fig. 1c)

$$E_{L,K} = \frac{\hbar^2}{6B\beta_0^2}\left[L(L+1) - K^2\right] + \left(n_\beta + \frac{1}{2}\right)\hbar\omega_\beta + (n_\gamma + 1)\hbar\omega_\gamma\,. \tag{9}$$

Here, $n_\beta$ is the number of $\beta$-oscillation quanta, $\omega_\beta$ is the frequency of $\beta$-oscillations, $n_\gamma$ is the number of $\gamma$-oscillation quanta, and $\omega_\gamma$ is the frequency of $\gamma$-oscillations.

### 3.2 Algebraic collective model

Experimental data allow identifying a sequence of collective states of a given nucleus that differ only in the values of some quantum numbers and are associated with large matrix elements of the quadrupole moment operator. These collective quadrupole excitations, if discussed only in terms of their energies, quadrupole moments, and electric quadrupole (E2) transitions, can be described by either five collective coordinates, as in the geometric approach in Section 3.1, or using creation and annihilation operators of quadrupole bosons in the algebraic approach to be discussed below. In the latter case, the problem is that the microscopic Hamiltonian of the nucleus depends on a large number of dynamical variables, among which the collective quadrupole variables are in no way singled out initially. Attempts have been made to construct a collective Hamiltonian as a series in powers of the bosonic operators, with only a small number of terms taken into account. But calculations have shown that these series poorly converge in practically interesting cases.

We consider a nucleus with even numbers of protons and neutrons. Because only states with even numbers of quasiparticles (elementary excitations of the fermionic-type ground state) are realized in such nuclei, we are interested only in the algebraic properties of the pair fermion operators $\alpha_s^+\alpha_t^+$, $\alpha_s^+\alpha_t$, and $\alpha_t\alpha_s$. Here, $\alpha_s^+$ ($\alpha_s$) is the creation (annihilation) operator of quasiparticles, introduced in the case of strong superfluidity-type pair correlations of nucleons in the nucleus. If pair correlations are weak, then the quasiparticles are given by the hole and particle states of valence nucleons. The pair fermionic operators generate a Lie algebra in the chosen configuration space [33, 38]:

$$\begin{aligned} A^+_{JMn} &= \frac{1}{\sqrt{2}}\sum_{s,s'}\psi^{Jn}_{ss'}(\alpha_s^+\alpha_{s'}^+)_{JM}\,,\\ A_{JMn} &= (A^+_{JMn})^+\,, \end{aligned} \tag{10}$$

where

$$(\alpha_s^+\alpha_{s'}^+)_{JM} = \sum_{m_s m_{s'}} C^{JM}_{j_s m_s j_{s'} m_{s'}}\alpha^+_{sm_s}\alpha^+_{s'm_{s'}}\,. \tag{11}$$

Here, $C^{JM}_{j_s m_s j_{s'} m_{s'}}$ is a Clebsch–Gordan coefficient, $s$ and $s'$ are the full sets of quantum numbers characterizing one-particle states except the projections of their angular momenta $m_s$ and $m_{s'}$ on the $z$-axis of the laboratory coordinate system, and $j_s$ and $j_{s'}$ are the angular momenta of nucleons in the $s$ and $s'$ states. The operators $A^+_{JMn}$ and $A_{JMn}$ are characterized by the angular momentum $J$, its projection $M$, and the additional quantum number $n$. The amplitudes $\psi^{Jn}_{ss'}$ satisfy the orthogonality relations

$$\begin{aligned} &\sum_{s,s'}\psi^{Jn}_{ss'}\psi^{Jn'}_{ss'} = \delta_{nn'}\,,\\ &\sum_{n}\psi^{Jn}_{ss'}\psi^{Jn}_{tt'} = \frac{1}{2}\left(\delta_{st}\delta_{s't'} - (-1)^{j_s+j_{s'}+J}\delta_{st'}\delta_{s't}\right). \end{aligned} \tag{12}$$

Using these relations, we can evaluate the commutator $[A_{JMn}, A^+_{J'M'n'}]$:

$$\begin{aligned} [A_{JMn}, A^+_{J'M'n'}] &= \delta_{JJ'}\delta_{MM'}\delta_{nn'}\\ &+ 2\sum_{ss't't'Lm}\psi^{Jn}_{ss'}\psi^{J'n'}_{st'}(-1)^{j_s+j_{s'}+J'+L}\sqrt{(2J+1)(2L+1)}\\ &\times\begin{Bmatrix} j_{s'} & j_s & J\\ J' & L & j_{t'}\end{Bmatrix} C^{J'M'}_{JMLm}(\alpha^+_{t'}\tilde{\alpha}_{s'})_{Lm}\,, \end{aligned} \tag{13}$$

where $(\alpha^+_t\tilde{\alpha}_{s'})_{Lm} = \sum_{m_t m_{s'}} C^{Lm}_{j_t m_t j_{s'} m_{s'}}\alpha^+_{tm_t}\alpha_{s'-m_{s'}}(-1)^{j_{s'}+m_{s'}}$. If we disregard the second term in the last commutator, then the operators $A_{JMn}$ and $A^+_{JMn}$ satisfy the commutation relations of bosonic creation and annihilation operators.

The set of operators $A_{JMn}$ and $A^+_{JMn}$ is only part of the entire Lie algebra. To close the algebra, we must extend the set by all their linearly independent commutators, i.e., $[A_{JMn}, A^+_{J'M'n'}]$. Using orthogonality relations (12), it can be shown that the set of operators $A_{JMn}$, $A^+_{JMn}$, and $[A_{JMn}, A^+_{J'M'n'}]$ is equivalent to the set of binary fermionic operators $\alpha_s^+\alpha_{s'}^+$, $\alpha_s\alpha_{s'}$, and $\alpha_s^+\alpha_{s'}$. Therefore, we can exactly express the nucleus Hamiltonian and all one-particle operators through the operators $A_{JMn}$, $A^+_{J'M'n'}$, and $[A_{JMn}, A^+_{J'M'n'}]$ [33, 38].

It is known from analyses of quadrupole excitations in nuclei in the random phase or the Tamm–Dancoff approximation that only one solution, with the lowest in energy and corresponding to one of the $A^+_{JMn}$ operators, specifically the

$A^+_{2Mn=1}$, is collective [39], i.e., generates a collective state by acting on the ground state of the nucleus. Other solutions are similar to two-quasiparticle ones in structure. Phases of the amplitude $\psi^{21}_{ss'}$ agree with the phases of the matrix elements of the quadrupole moment operator [39], and therefore matrix elements of electric quadrupole transitions are coherently enhanced. The algebra of collective quadrupole operators includes $A^+_{2M1}$, $A_{2M1}$, and their commutator.

Let us consider the double commutator [33]

$$\left[[A_{2M1}, A^+_{2M'1}], A^+_{2M''1}\right] = -K(\delta_{MM'}A^+_{2M''1} + \delta_{MM''}A^+_{2M'1}) - \sum_{L,n\neq 1} K^{Ln}_{MM'M''M'''}A^+_{LM'''n}, \quad (14)$$

where $M$, $M'$, $M''$, and $M'''$ are values of the angular momentum projection characterizing the corresponding operators, and the coefficient $K^{Ln}_{MM'M''M'''}$ is the sum of products of two Clebsch–Gordan coefficients, two $6j$ symbols, and four amplitudes $\psi^{Ln}_{ss'}$. The coefficient $K$ can be expressed through the amplitudes $\psi^{21}_{ss'}$. We see that, strictly speaking, the algebra of operators $A_{2M1}$, $A^+_{2M1}$, and $[A_{2M1}, A^+_{2M'1}]$ is not closed. However, first, the coefficients $K^{Ln}_{MM'M''M'''}$ with $Ln \neq 21$ do not contain coherent terms and are therefore small. Second, if we are interested in only the matrix elements of the double commutator that relate to collective states, then the contribution of noncollective operators can be ignored in view of its smallness. In that approximation, the operators $A_{2M1}$, $A^+_{2M1}$, and $[A_{2M1}, A^+_{2M'1}]$ generate a closed algebra, and it can be shown that this is the SU(6) algebra [33]. For the operators $A_{2M1}$, $A^+_{2M1}$, and $[A_{2M1}, A^+_{2M'1}]$, we then have the following representations in terms of bosonic operators:

$$A^+_{2M1} \to d^+_{2M}\sqrt{1 - \frac{1}{N}\sum_v d^+_{2v}d_{2v}} \to d^+_{2M}\, s\, \frac{1}{\sqrt{N}},$$
$$A_{2M1} \to \sqrt{1 - \frac{1}{N}\sum_v d^+_{2v}d_{2v}}\, d_{2M} \to s^+ d_{2M}\, \frac{1}{\sqrt{N}}, \quad (15)$$
$$[A_{2M1}, A^+_{2M'1}] \sim d^+_{2M'}d_{2M},$$

where $N$ is a positive number specifying the maximum number of bosons that can be generated by $A^+_{2M1}$ and characterizing the SU(6) representation (the value of $N$ being determined by the coefficient $K$); $d^+_M$ ($d_M$) is the creation (annihilation) operator of the quadrupole boson with the angular momentum projection $M$; and $s^+$ ($s$) is the creation (annihilation) operator of the monopole boson. The collective Hamiltonian of the nucleus can be constructed using approximate expressions for pair fermionic operators in terms of $A_{2M1}$, $A^+_{2M1}$, and $[A_{2M1}, A^+_{2M'1}]$. This Hamiltonian has the form [33, 38]

$$H_{\text{coll}} = \varepsilon\sum_\mu d^+_{2\mu}d_{2\mu} + \kappa_1\left(\sum_\mu d^+_{2\mu}(-1)^\mu d^+_{2-\mu}ss + \text{h.c.}\right) + \kappa_2\left(\sum_\mu (d^+_2 d^+_2)_{2\mu}d_{2\mu}s + \text{h.c.}\right) + \frac{1}{2}\sum_{L=0,2,4} C_L \sum_M (d^+_2 d^+_2)_{LM}(d_2 d_2)_{LM}, \quad (16)$$

where the parentheses $(\ldots)_{LM}$ denote vector coupling. The six constants entering Hamiltonian (16) are functions of the amplitudes $\psi^{21}_{ss'}$, i.e., of the one-quasiparticle energies and the parameters characterizing the effective interaction of nucleons in the nucleus. In principle, they can be calculated within some microscopic model of the nucleus, but in the overwhelming majority of studies they are taken as fitting parameters.

For simplicity and compactness of the formulas, the above expressions for collective operators in terms of binary fermionic operators are given in the Tamm–Dancoff approximation. A more general analysis using the random phase approximation can be done similarly. In the general case, along with the amplitudes $\psi^{21}_{ss'}$, the so-called backward amplitudes $\phi^{21}_{ss'}$ are also introduced [33].

Considering all the 36 operators generating the U(6) algebra, namely, $d^+_{2\mu}s$, $s^+d_{2\mu}$, $d^+_{2\mu}d_{2\mu'}$, and $s^+s$, we see that some of these operators generate subalgebras. We can select three chains of subalgebras [32]:

$$\begin{aligned}&\text{U}(6) \supset \text{U}(5) \supset \text{O}(5) \supset \text{O}(3) \supset \text{O}(2),\\ &\text{U}(6) \supset \text{O}(6) \supset \text{O}(5) \supset \text{O}(3) \supset \text{O}(2),\\ &\text{U}(6) \supset \text{SU}(3) \supset \text{O}(3) \supset \text{O}(2).\end{aligned} \quad (17)$$

In the general case, the Hamiltonian has to be diagonalized numerically, but there are still cases where the eigenvalue problem can be solved analytically: in cases of dynamical symmetries, which had played a major role in working out the algebraic collective model of the nucleus. These cases occur when the Hamiltonian can be represented as a sum of the Casimir operators for the groups entering one of the subalgebra chains in (17). For the first chain, the eigenfunctions of the Hamiltonian are simultaneously eigenfunctions of the particle number operator of quadrupole bosons. This case is equivalent to the limit of a spherical nucleus in the geometric collective model. Depending on the parameters of the Hamiltonian, the spectrum of excited states consists of degenerate or split multiplets of quadrupole bosons. Because the maximum number of quadrupole bosons is bounded, the spectrum of such a Hamiltonian consists of finitely many excited states, in contrast to the spectrum of the geometric collective model.

In the case of the second reduction chain, eigenfunctions of the Hamiltonian are no longer eigenfunctions of the number-of-bosons operator and the state spectrum is similar to the excitation spectrum of a $\gamma$-soft nonaxial rotor in the geometric collective model.

In the third case, the spectrum of excited states of the Hamiltonian consists of rotational bands, as in the case of the axially symmetric Hamiltonian for the rotor in the geometric collective model.

In the framework of the algebraic collective model, we have thus obtained the same three limit cases of the nucleus shape and the spectrum of excited states as in the geometric collective model.

## 4. Description of phase transitions in the algebraic collective model of the nucleus

In this section, we outline the general strategy for considering phase transitions between different shapes of a nucleus in the framework of the model of interacting bosons. In Sections 5 and 6, we discuss the geometric collective model.

Like any model with a definite group structure, the model of interacting bosons is closely related to the internal geometric structure of the nucleus, which highlights its

similarity to the geometric collective model. At the same time, the Hamiltonian of the model of interacting bosons has a very simple algebraic structure, which allows obtaining many results analytically.

The study of the geometric properties of the model of interacting bosons is associated with the introduction of coherent states into consideration [40–43]. For our purposes, it is convenient to work in terms of the so-called projective coherent states, which are given by

$$|N;\alpha_\mu\rangle = \left(s^+ + \sum_\mu \alpha_\mu d_\mu^+\right)^N |0\rangle\,. \tag{18}$$

Here, $N$ is the maximum number of bosons characterizing a given representation of U(6), typically set equal to half the number of valence nucleons in the chosen nucleus; the state vector $|0\rangle$ is the bosonic vacuum; and $\alpha_\mu$ are directly related to the variables describing the nucleus shape. As in Section 3, instead of the five variables $\alpha_\mu$, we can use the three Euler angles $\boldsymbol{\Omega} \equiv (\theta_1, \theta_2, \theta_3)$ and two internal variables characterizing the nucleus shape, $\beta$ and $\gamma$:

$$\alpha_\mu = \sum_\nu D^2_{\mu\nu}(\theta_1, \theta_2, \theta_3) a_\nu\,, \tag{19}$$

where $a_0 = \beta\cos\gamma$, $a_{\pm 2} = (1/\sqrt{2})\beta\sin\gamma$, and $a_{\pm 1} = 0$. Thus, a normalized coherent state can be expressed as

$$|N;\beta,\gamma\rangle = \frac{1}{\sqrt{N!(1+\beta^2)^N}}(B^+)^N|0\rangle\,, \tag{20}$$

where

$$B^+ = s^+ + \beta\left[d_0^+\cos\gamma + \frac{1}{\sqrt{2}}(d_2^+ + d_{-2}^+)\sin\gamma\right]. \tag{21}$$

We introduce the Hamiltonian that is frequently used in investigations based on the model of interacting bosons [32]:

$$\hat{H}(N,\xi,\chi) = (1-\xi)\hat{n}_d - \frac{\xi}{N}\,\hat{Q}^\chi\hat{Q}^\chi\,. \tag{22}$$

Here, $\hat{n}_d \equiv \sum_\mu d_\mu^+ d_\mu$ is the particle number operator of quadrupole bosons, and the quadrupole moment operator $\hat{Q}^\chi$ is

$$\hat{Q}^\chi_\mu = d_\mu^+ s + s^+\bar{d}_\mu + \chi(d^+\bar{d})_{2\mu}\,,\quad \bar{d}_\mu = (-1)^\mu d_{-\mu}\,. \tag{23}$$

The parameters $\xi$ and $\chi$ play the role of control parameters, similarly to the temperature and pressure in thermodynamics. The $\xi$ parameter takes values between zero and one, $\xi \in [0,1]$. At $\xi = 1$, we have the limit case of a nucleus with quadrupole deformation, which includes the cases of a prolate axially symmetric nucleus, an oblate axially symmetric nucleus, and a nucleus with broken axial symmetry. At $\xi = 0$, we have the limit case of a spherical nucleus, described by the five-dimensional harmonic oscillator. The $\chi$ parameter ranges as $\chi \in [-\sqrt{7}/2, \sqrt{7}/2]$. At $\xi = 1$ and $\chi = -\sqrt{7}/2$, we have the case of a prolate deformed nucleus, and at $\xi = 1$ and $\chi = \sqrt{7}/2$, the case of an oblate deformed nucleus. In both cases, the nucleus has axial symmetry. At $\xi = 1$ and $\chi = 0$, the energy of the nucleus is unchanged as its shape changes from prolate to oblate. From the group theory standpoint, at $\xi = 0$ we have the case of U(5) dynamical symmetry, at $\xi = 1$ and $\chi = -\sqrt{7}/2$, the case of SU(3) dynamical symmetry, at $\xi = 1$ and $\chi = \sqrt{7}/2$, $\overline{\mathrm{SU(3)}}$ dynamical symmetry [44], and at $\xi = 1$ and $\chi = 0$, O(6) dynamical symmetry.

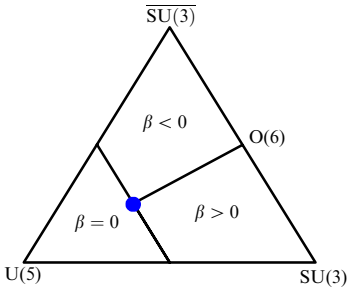


**Figure 2.** Phase diagram of the model of interacting bosons. The dot in the center of the triangle shows the triple point, at the junction of the spherical and two deformed phases. The $\xi$ parameter in Hamiltonian (22) changes in the direction from the U(5) point to the O(6) point. Along this direction, the parameter $\chi$ of the quadrupole moment operator is equal to zero. The $\chi$ parameter changes along the direction defined by the line connecting the SU(3) and $\overline{\mathrm{SU(3)}}$ points. On this line, $\xi = 1$. At the U(5) point, $\xi = 0$.

In the literature on the model of interacting bosons, the two-dimensional space defined by the parameters $\xi$ and $\chi$ is represented by an extended Casten triangle [45], shown in Fig. 2, where $\xi$ varies along the direction from the U(5) point to the O(6) point. Along this direction, $\chi = 0$. The $\chi$ parameter varies along the direction of the line connecting the SU(3) and $\overline{\mathrm{SU(3)}}$ points. On that line, $\xi = 1$. At the U(5) point, $\xi = 0$. Instead of the thermodynamical potential used in classical physics, we analyze the mean value of Hamiltonian (22) in coherent state (18) as a function of the control parameters $\xi$ and $\chi$ [46]:

$$\begin{aligned} E(N,\xi,\chi;\beta,\gamma) &\equiv \langle N;\beta,\gamma|\hat{H}(N,\xi,\chi)|N;\beta,\gamma\rangle \\ &= -5\xi + \frac{1}{(1+\beta^2)^2}\left\{\left(N(1-\xi) - \xi(4N+\chi^2-8)\right)\beta^2\right. \\ &\quad + 4(N-1)\xi\sqrt{\frac{2}{7}}\chi\beta^3\cos(3\gamma) \\ &\quad \left. + \left[N(1-\xi) - \xi\left(\frac{2N+5}{7}\,\chi^2 - 4\right)\right]\beta^4\right\}. \end{aligned} \tag{24}$$

The problem is to minimize the energy functional $E(N,\xi,\chi;\beta,\gamma)$ by varying $\beta$ and $\gamma$ for each value of $\xi$ and $\chi$. The simple dependence on $\gamma$ in (24) allows us to easily find the value of $\gamma$ that corresponds to a minimum of $E(N,\xi,\chi;\beta,\gamma)$. When $\chi < 0$, the minimum is at $\gamma = 0$, and when $\chi > 0$, at $\gamma = \pi/3$. In the general case, $\chi\cos(3\gamma) = -|\chi|$.

We regard the value of the energy functional at the global minimum point as an approximate value of the ground state energy of the nucleus. This last quantity is a continuous function of the control parameters $\xi$ and $\chi$, although the position of the global minimum on the plane of $\beta$ and $\gamma$ can change jump-wise. However, the derivatives $E(N,\xi,\chi;\beta,\gamma)$ with respect to the control parameters can have discontinuity points. Discontinuities of the first- and second-order derivatives correspond to respective first- and second-order phase transitions.

Landau's approach [47] is entirely applicable to the analysis of phase transitions among different shapes of the nucleus in the model of interacting bosons, i.e., to the analysis of the energy functional $E(N,\xi,\chi;\beta,\gamma)$. Expanding (24) in a series in powers of $\beta$ and setting $\gamma = 0$, we

obtain

$$E(N,\xi,\chi;\beta,\gamma=0)=-5\xi+\left[N(1-\xi)-\xi(4N+\chi^2-8)\right]\beta^2 - 4(N-1)\xi\sqrt{\frac{2}{7}}|\chi|\beta^3 + \left[\xi\left(8N-\frac{2N-9}{7}\chi^2-12\right)-N(1-\xi)\right]\beta^4+\ldots. \quad (25)$$

The equilibrium configuration changes the value of $\beta$ from $\beta=0$ to $\beta\neq 0$ if the coefficient at $\beta^2$ changes from positive to negative. Therefore, this coefficient vanishes at the phase transition point. For the phase transition point to be stable, the coefficient at $\beta^3$ must also vanish in it. But this is possible only if $\chi=0$. At $\chi=0$, the coefficient at $\beta^2$ vanishes if $\xi\equiv\xi_{\text{trip}}=N/(5N-8)$. These values of $\xi$ and $\chi$ are coordinates of the so-called triple point inside the Casten triangle (see Fig. 2), located at the junction of the spherical phase ($\beta=0$) belonging to the domain $\xi<\xi_{\text{trip}}$ and two deformed phases occurring for $\xi>\xi_{\text{trip}}$. We note that, if $\chi<0$, then the nucleus is prolate, and if $\chi>0$, it is oblate. Two deformed phases are separated by the line $\chi=0$. In the rest of the Casten triangle, except at the triple point, phase transitions between spherical and deformed phases and between two deformed phases are first-order phase transitions in this model.

At $\chi\neq 0$, the transition from the deformed phase to the spherical one occurs as follows. As $\xi$ decreases from $\xi=1$ and reaches the value $\xi=N/(5N+\chi^2-8)$, the energy functional $E(N,\xi,\chi;\beta,\gamma)$ acquires a minimum at $\beta=0$. But, at the beginning, this is only a local minimum. The global minimum remains at $\beta\neq 0$. As $\xi$ decreases further, the depths of the spherical and deformed minima equalize. For $\chi\neq 0$ and some values of $\xi$, we thus have an energy functional with two minima. This implies that the spherical and deformed phases can coexist for $\chi\neq 0$. On the other hand, two minima do not occur at the triple point [48]. As regards the transition from the oblate to the deformed prolate shape, no two-minimum pattern occurs either. The position of the minimum in $\gamma$ changes jump-wise from $\gamma=0$ to $\gamma=\pi/3$ under the change of sign of $\chi$.

## 5. Phase transition from spherical to deformed shape in nuclei at the beginning of the rare-earth range

A well-known and experimentally studied example of nuclei exhibiting a transition from a spherical to a deformed shape is given by isotopes of Nd, Sm, Gd, and Dy. As the number of neutrons increases, the spectra of low-lying excited states of these nuclei undergo a transition from the typically vibrational spectrum to a typical rotational one.

From Table 1, which gives experimental values of the ratio $R_{4/2}$ for different numbers of neutrons in isotopes of these elements, we see that $R_{4/2}$ sharply increases for $N\geqslant 90$ neutrons, indicating that the transition from the spherical to the deformed shape in isotopes of Nd, Sm, Gd, and Dy occurs at $N=90$.

The transition from the spherical to the deformed shape in isotopes of Nd, Sm, Gd, and Dy is probably a second-order phase transition, because in most of the calculations the potential energy of the deformation of these nuclei has only one minimum as a function of the deformation parameter, and the energy of the nucleus at the minimum is a monotonically decreasing function of the degree of deformation at the minimum; hence, the first derivative experiences no jump.

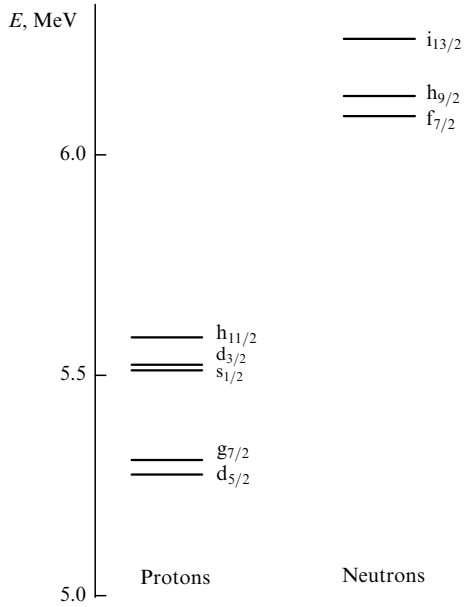


**Figure 3.** Part of the arrangement of spherical single particle levels in the shell model of the nucleus ($Z>50$, $N>82$).

**Table 1.** Values of $R_{4/2}$ in isotopes* of Nd, Sm, Gd, and Dy.

| Z \ N | 84 | 86 | 88 | 90 | 92 | 94 | 96 |
|---|---|---|---|---|---|---|---|
| $_{60}$Nd | 1.89 | 2.30 | 2.49 | 2.93 | 3.27 | 3.29 | 3.31 |
| $_{62}$Sm | 1.85 | 2.14 | 2.32 | 3.08 | 3.28 | 3.29 | 3.30 |
| $_{64}$Gd | 1.81 | 2.02 | 2.19 | 3.01 | 3.24 | 3.29 | 3.30 |
| $_{66}$Dy | 1.81 | 2.05 | 2.24 | 2.93 | 3.21 | 3.27 | 3.29 |

*Experimental data are taken from [56].

In [49], however, it was hypothesized that the phase transition in nuclei we considered is still a first-order phase transition, and the quadrupole deformation of the nuclei occurs due to the following mechanism. In the nuclei under consideration, protons fill the single particle levels $d_{5/2}$ and $g_{7/2}$ (Fig. 3). The next single particle level $h_{11/2}$ is separated from $d_{5/2}$ and $g_{7/2}$ by an energy gap. At values of $N$ starting at $N=90$, neutrons fill the single particle state $h_{9/2}$, in which they strongly interact with protons if the latter are in the $h_{11/2}$ state. Therefore, the nucleus gains in energy if protons start filling the $h_{11/2}$ state. As a result, the binding energy of a proton in the $h_{11/2}$ state increases, and the energy gap between the single particle proton states $d_{5/2}$ and $g_{7/2}$, on the one hand, and $h_{11/2}$, on the other hand, sharply decreases. The space of single particle states that can be occupied by valence protons increases, which enhances the collective effects in the motion of nucleons and helps create the deformation.

This argument, however, is based on the model of single particle levels of a spherical nucleus and does not involve changes in the mean field due to deformation [50]. As a result of the deformation of the mean field of the nucleus, the role of specific proton and neutron single particle levels also changes, but the order of filling these states is essential for the realization of the Federman–Pittel mechanism. At $N=90$, neutrons find it energetically advantageous to occupy the single particle level $i_{13/2}$. Due to a larger orbital momentum in that state and the associated large magnitude of the quad-

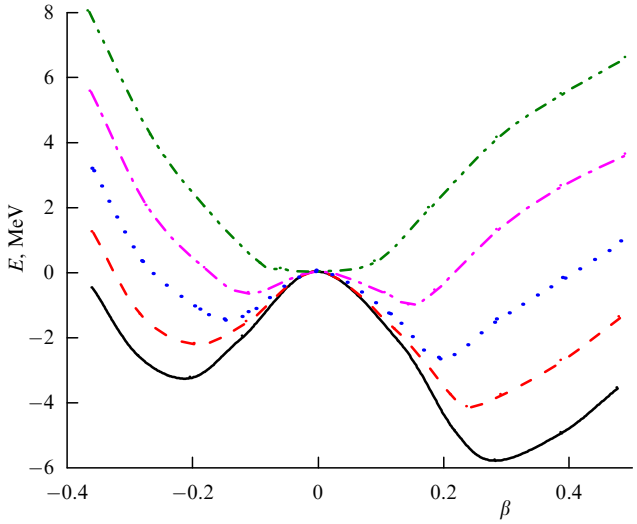


**Figure 4.** Example of the evolution of the potential energy of nucleus deformation at the beginning of the rare-earth domain as the number of neutrons increases. A spherical nucleus corresponds to the dashed-double-dotted line. The solid line shows a strongly deformed axially symmetric nucleus. The dashed-dotted, dotted, and dashed lines correspond to transitional nuclei with increasing quadrupole deformation.

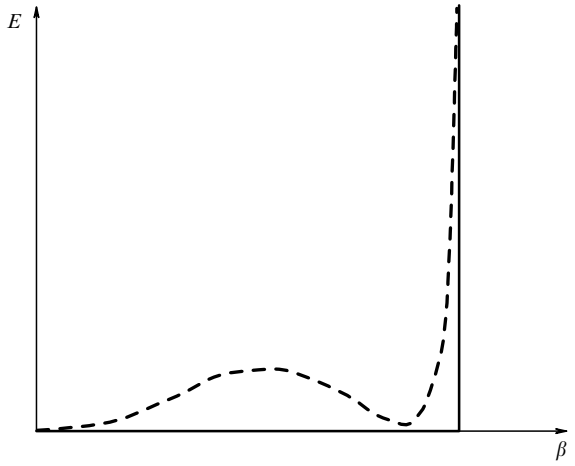


**Figure 5.** Example of the deformation potential energy for a transitional nucleus (dashed line) and the rectangular well potential of infinite depth.

rupole moment, the equilibrium deformation of the nucleus smoothly grows starting from zero, and the deformation energy of the nucleus at the minimum smoothly changes as the $i_{13/2}$ states are being filled with neutrons. Although the number of neutrons in a nucleus is a discrete quantity, this can be formally regarded as an indication that the derivative of the deformation energy of the nucleus at the minimum with respect to the deformation parameter changes smoothly. A major part of the calculations of the potential energy of deformation for the nuclei in question also suggests that, as the number of neutrons increases, the potential energy in the nucleus at the beginning of the rare-earth domain evolves, as is shown in Fig. 4.

We next discuss the experimental data. In $^{150}$Nd, $^{152}$Sm, and $^{154}$Gd nuclei, low-lying $0_2^+$ and $2_2^+$ states are known that are associated with strong E2-transitions. But the probabilities of these transitions are comparable to the probabilities of $2_1^+ \to 0_1^+$ transitions, and the E2-transition $2_2^+ \to 0_2^+$ in $^{154}$Gd is three times weaker than the $2_1^+ \to 0_1^+$ transition. Therefore, it would be groundless to assume that the relevant nuclei, for example, are deformed more strongly in the $2_2^+$ and $0_2^+$ states than in the $2_1^+$ and $0_1^+$ states. If these E2 transitions differed greatly in their magnitude, we would be able to speak of the coexistence of states characterized by different nucleus shapes at different excitation energies in the same nucleus. This would then suggest that in $^{150}$Nd, $^{152}$Sm, and $^{154}$Gd nuclei, the transition from the spherical to the deformed shape can be regarded as a first-order phase transition. However, it is not impossible that, although the potential energy of these nuclei has two minima, the amplitude of oscillations in $\beta$ is large, and the wave functions of collective states are not localized in one of the minima. In [51], a simple analytic model for just this case is proposed.

In [51, 52], a simple description is given for transitional nuclei within the geometric model of the nucleus, based on potentials of a simple shape, which allows obtaining an analytic solution to the problem. The main idea in [51, 52] is illustrated in Fig. 5, where the dashed line shows the potential energy of a nucleus that is transitional between spherical and deformed nuclei. This potential has two minima that correspond to the spherical and deformed shapes of the nucleus but are separated by a moderate barrier; the potential sharply increases under deformations exceeding the deformation in the second minimum. Iachello [51] suggested approximating such a potential with a rectangular infinitely deep well (solid line in Fig. 5), which, evidently, is somewhat of an oversimplification, but the results of the calculation turned out to be close to the experimental data for transitional nuclei at the beginning of the rare-earth domain. Based on such a potential, it was proposed to consider two cases that differ in how the potential depends on $\gamma$. In the first case, the proposal was that, as a function of $\gamma$, the potential has a deep minimum at $\gamma = 0$, and in the second case a potential independent of $\gamma$ was considered. Together with the assumption that the $\beta$ and $\gamma$ variables separate, this leads to an analytic solution of the Schrödinger equation with Bohr's Hamiltonian. In both cases, the eigenfunction of Bohr's Hamiltonian is factored:

$$\Psi(\beta, \gamma, \boldsymbol{\Omega}) = f(\beta)\varphi(\gamma, \boldsymbol{\Omega})\,. \tag{26}$$

In the first case, the function $f(\beta)$ is a solution of the differential equation

$$\left[-\frac{1}{\beta^4}\frac{\partial}{\partial\beta}\beta^4\frac{\partial}{\partial\beta} + \frac{1}{3\beta^2}I(I+1) + u(\beta)\right] f(\beta) = \varepsilon_\beta f(\beta)\,, \tag{27}$$

where $u(\beta) = 0$ for $\beta \leqslant \beta_\mathrm{b}$ and $u(\beta) = \infty$ for $\beta > \beta_\mathrm{b}$, with $\beta_\mathrm{b}$ being the width of the potential well. The function $\varphi(\gamma, \boldsymbol{\Omega})$ has the form $\varphi(\gamma, \boldsymbol{\Omega}) = \eta_K(\gamma) D^I_{MK}(\boldsymbol{\Omega})$, where $\eta_K(\gamma)$ is a solution of the equation

$$\left[-\frac{1}{\langle\beta^2\rangle}\frac{1}{\gamma}\frac{\partial}{\partial\gamma}\gamma\frac{\partial}{\partial\gamma} + \frac{(K/2)^2}{\langle\beta^2\rangle}\frac{1}{\gamma^2} + \frac{1}{2}C_\gamma\gamma^2\right]\eta_K(\gamma) = \varepsilon_\gamma\eta_K(\gamma)\,, \tag{28}$$

$\langle\beta^2\rangle$ being the effective value of $\beta^2$ formed as a consequence of the assumption about the separation of $\beta$ and $\gamma$ variables. Equation (27) is solved by the function $\beta^{-3/2}J_\nu(x_{sI}\beta/\beta_\mathrm{b})$, where $J_\nu$ is the Bessel function, $x_{sI}$ is its $s$th zero, and $\nu = \sqrt{(1/3)I(I+1) + 9/4}$. In this case, the ratio of the lowest $4_1^+$ and $2_1^+$ state energies $R_{4/2} \equiv E(4_1^+)/E(2_1^+) = 2.91$ is just between the values characteristic of spherical ($R_{4/2} = 2.0$) and axially deformed ($R_{4/2} = 3.33$) nuclei. The

key result is the value $R_{0/2} \equiv E(0_2^+)/E(2_1^+) = 5.67$ predicted in the approximation under consideration. This result is independent of the parameters of the Hamiltonian. In the transitional nucleus $^{152}$Sm, this ratio is 5.62. Numerous other experimental results pertaining to excitation energies and probabilities of electric quadrupole (E2) transitions in $^{150}$Nd, $^{152}$Sm, and $^{154}$Gd also turned out to be close to the results obtained in this approximation. Significant deviations of theoretical results from experimental data were found for the E2 transitions between states belonging to different quasirotational bands, i.e., bands based on the ground $(0_1^+)$ state and the $0_2^+$ and $2_3^+$ states. It was shown in [53], however, that the agreement with experimental data is strongly improved if the difference in the values of the coefficient of inertia for rotational and vibrational modes is taken into account.

If we assume that the potential energy is independent of $\gamma$, then the function $f(\beta)$ satisfies the equation

$$\left[-\frac{1}{\beta^4}\frac{\partial}{\partial\beta}\beta^4\frac{\partial}{\partial\beta}+\frac{v(v+3)}{\beta^2}+u(\beta)\right]f(\beta)=\varepsilon f(\beta)\,, \qquad (29)$$

where $u(\beta)$ has the same shape as in the preceding case. The solution of Eqn (29) has the form $\beta^{-3/2}J_{v+3/2}(x_{sv},\beta/\beta_b)$, where $x_{sv}$ is the $s$th zero of the Bessel function $J_{v+3/2}$ and $v$ is the seniority of the state (see (5)). The spectrum of eigenstates of Eqn (29) and the ratios of probabilities of E2 transitions obtained with the use of eigenfunctions of this equation are close to the corresponding experimental data for some isotopes of Xe and Ba [54].

## 6. Phase transitions and shape coexistence in nuclei with about 100 nucleons

Quantum phase transitions discovered in atomic nuclei can be divided into two groups. The first contains transitions in those nuclei whose mean fields have only one stable configuration for any values of the control parameters. In other words, the potential energy of the nucleus has only one minimum, which, however, can be responsible for both spherical and deformed shapes, depending on the values of control parameters. The control parameters can include the numbers of protons and neutrons. In that case, the phase transition, i.e., a change in the mean field symmetry, occurs as the numbers of protons and neutrons change.

The second group contains transitions in nuclei whose mean fields, depending on many dynamical variables, have two stable configurations with different mean field symmetries and total energies. In that case, the phase transition from one configuration to the other occurs as the excitation energy of the nucleus changes.

Both types of phase transitions were discussed in Section 5 in relation to phase transitions from spherical nuclei at the beginning of the rare-earth domain to deformed nuclei. We gave both interpretations, although the majority of researchers tend to assign phase transitions in those nuclei to the first group. In this section, we consider the case of the $^{96}$Zr nucleus, where the phase transition occurring as the excitation energy increases belongs to the second group.

Atomic nuclei with the mass number $A \sim 100$ are nuclei in which states characterized by a spherical or deformed shape coexist. The transition from one nucleus shape to another occurs as the excitation energy increases. The class of such nuclei comprises isotopes of Sr, Zr, and Mo (see the references in [10, 55]). As an example, we consider Zr isotopes in which, from the standpoint of the single particle shell model, protons fill the $p_{1/2}$ state, and the single particle proton state $g_{9/2}$ that is next in energy is separated from $p_{1/2}$ by an energy gap, such that Zr can also be regarded as a semimagic nucleus. The number of valence neutrons in light isotopes of Zr is not high.

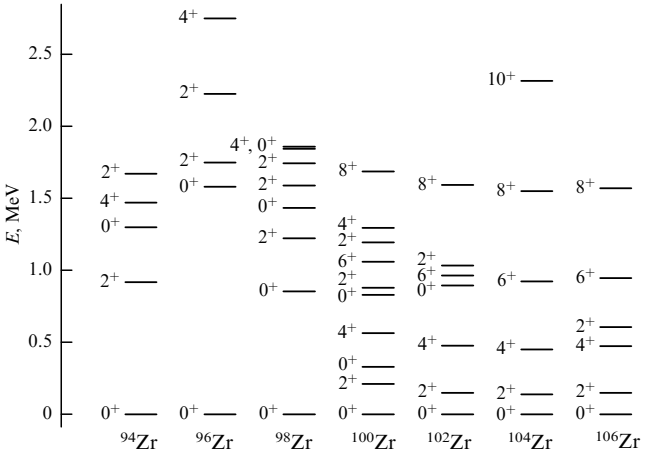


**Figure 6.** Experimental spectra of $^{94-106}$Zr nuclei.

In Fig. 6, we give experimental spectra of the low-lying states of $^{96-106}$Zr [56]. We can see that, among the low-lying states in $^{96-100}$Zr, there is the excited $0^+$-state $(0_2^+)$. The probabilities of E2 transitions between the first excited $2^+$ state $(2_1^+)$ and the ground state in $^{96-98}$Zr are characteristic of transitions in spherical nuclei and amount to several one-particle units (Weisskopf units) (2–6 W.u.) [56]. At the same time, the reduced probability of the E2 transition $B(\mathrm{E2}; 2_2^+ \to 0_2^+)$ measured in $^{96}$Zr is 36 W.u. Such a large value is characteristic of deformed nuclei. This suggests that in light isotopes of Zr the ground state $(0_1^+)$ and the $2_1^+$ state are characterized by a spherical shape, whereas the $0_2^+$ and $2_2^+$ states are deformed ones. The situation changes dramatically in $^{100}$Zr, where $B(\mathrm{E2}; 2_1^+ \to 0_1^+) = 75$ W.u. Such a large value of the E2-transition probability is characteristic of deformed nuclei. In addition, the relation of energy intervals in the band based on the ground state of $^{100}$Zr $(0_1^+, 2_1^+, 4_1^+, 6_1^+)$ suggests the rotational character of these states, which also is evidence that the ground state of this nucleus is deformed.

The following pattern therefore transpires. The ground state of light isotopes of Zr is spherical, but already at moderate excitation energies, the deformed $0_2^+$ state exists in these nuclei. As the number of valence nucleons increases, the deformed state goes down in energy and becomes the ground state in $^{100}$Zr. The mechanism conducive to the appearance of deformation in the ground state is in this case the Federman–Pittel mechanism. When the valence neutrons start filling the single particle state $g_{7/2}$, the next one after $d_{5/2}$, it becomes energetically advantageous for the nucleus that the protons simultaneously occupy the single particle state $g_{9/2}$, the next one after $p_{1/2}$. It is known that protons in the $g_{9/2}$ state and neutrons in the $g_{7/2}$ state strongly interact due to tensor forces [23]. Hence, the binding energy of neutrons in the $g_{7/2}$ state increases, and it drops in energy in the single particle spectrum of the nucleus. The space of single particle states available to valence neutrons sharply expands, which enhances the collective quadrupole mode, increasing the amplitude of collective quadrupole motion. In addition, the single particle $g_{9/2}$ state occupied with protons is characterized by a large

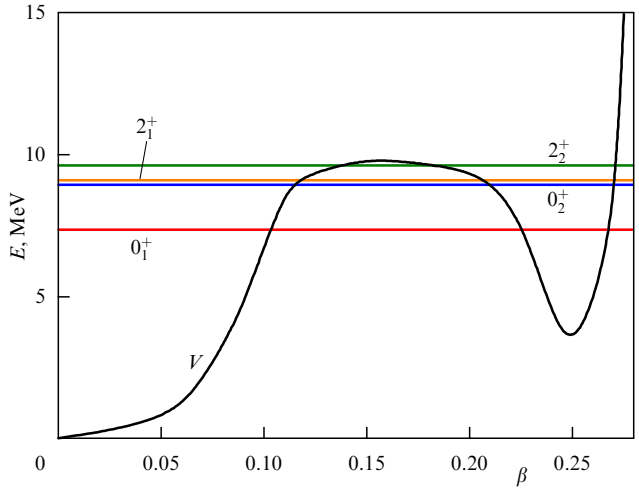


**Figure 7.** (Color online.) Potential energy $V(\beta)$ and the calculated energy levels for the $^{96}$Zr nucleus [59].

quadrupole moment, which also facilitates the deformation of the nucleus. Due to this mechanism, the deformed excited state exists in light isotopes of Zr. However, because the transition of neutrons from the $d_{5/2}$ to the $g_{7/2}$ state requires additional excitation energy, the deformed state is realized at a higher energy than the spherical one.

The most exhaustive collection of experimental data on low-lying collective quadrupole excitations has been obtained for $^{96}$Zr [57]. We consider this nucleus within the geometric collective model. Obviously, interpreting the coexistence of differently shaped states in a nucleus is the task of a microscopic theory. But the collective model in which variable shapes of the nucleus are directly used as dynamical variables allows describing dynamical consequences of the coexistence of shapes in the simplest way. In addition, it is of interest to see to what degree the collective model can reproduce the experimental data.

A sharp change in the shape of the ground state in isotopes of Zr is an exception. However, the mixing of spherical and deformed components is possible in wave functions of eigenstates of the nucleus. It is therefore interesting how strong this mixing is. This question can be analyzed in the framework of the collective model of the nucleus. Data on E2 transitions between excited states [58] suggest that spherical and deformed states in $^{96}$Zr are very pure.

In Ref. [59], the properties of $^{96}$Zr are studied within the collective model with a potential having two minima (Fig. 7), spherical and deformed. An analogue of this picture in the algebraic model of the nucleus is the treatment in the bosonic space embracing configurations with different values of the maximum number of bosons, namely, $N$ and $N+2$. To simplify the problem, it was assumed that the $\gamma$ variable can be separated from $\beta$ in the Hamiltonian. This assumption was also justified by the fact that experimental data give no indication of the existence, among low-lying states, of those that are explicitly related to excitations in $\gamma$. It was also assumed that $\gamma$ oscillates with a moderate amplitude about $\gamma = 0$. The results of the calculation are given in Table 2. As we can see, the obtained results are in good correspondence with experimental data.

We note the following, however. In [60, 61], as a result of analyzing experimental data on rotational and vibrational states of deformed nuclei, it was shown that the coefficient of inertia for rotational motion is several times smaller than the

**Table 2.** Results of calculating energies and reduced probabilities for electromagnetic transitions* for $^{96}$Zr.

| Energies and transition probabilities | Calculation | Experiment |
|---|---|---|
| $E(2_1^+)$ | 1748 | 1750 |
| $E(2_2^+)$ | 2268 | 2226 |
| $E(0_2^+)$ | 1582 | 1582 |
| $B(\mathrm{E2}; 2_2^+ \to 0_2^+)$ | 26.1 | 36(11) |
| $B(\mathrm{E2}; 2_1^+ \to 0_1^+)$ | 3.6 | 2.3(3) |
| $B(\mathrm{E2}; 2_2^+ \to 0_1^+)$ | 0.26 | 0.26(8) |
| $\rho^2(0_2^+ \to 0_1^+)$ | 0.0013 | 0.0075 |
| $B(\mathrm{E2}; 2_2^+ \to 2_1^+)$ | 2.25 | $2.8^{+1.5}_{-1.0}$ |
| $B(\mathrm{E2}; 2_1^+ \to 0_2^+)$ | 6.8 | — |
| $B(\mathrm{M1}; 2_2^+ \to 2_1^+)$ | 0.11 | 0.14(5) |
| $Q(2_2^+)$ | − 0.51 | — |

* The value of $b_{\mathrm{rot}}$ characterizing the ratio of rotational-to-vibration coefficients of inertia is taken equal to 0.2. The values $B$(E2) are expressed in units of W.u., and of $B$(M1), in nuclear magnetons. The value $Q(2_2^+)$ is expressed in $e$ bn. Excitation energies are expressed in keV. The dimensionless quantity $\rho^2 2(0_2^+ \to 0_1^+)$ characterizes the electric monopole transition between $0_2^+$ and $0_1^+$ states. The experimental energy of the $0_2^+$ state is used to fix $B_0$. Experimental data are taken from [58].

coefficient of inertia for the vibration mode. Taking this into account has allowed obtaining a good description of the $2_2^+$ state energy in $^{96}$Zr.

The calculation of $B(\mathrm{M1}; 2_2^+ \to 2_1^+)$ within the geometric collective model leads to a result three orders of magnitude smaller than the experimental value. It was therefore taken into account in [59] that the calculation within the shell model, done under the assumption of a spherically shaped nucleus, leads to a negative value of the $g_R$ factor, namely, to $g_R = -0.26$, in contrast to the $g_R$ factor equal to $Z/A$ in the geometric collective model with only the contribution of the orbital motion of protons to the magnetic moment taken into account. We note that the result obtained within the shell model was expected because, in the case of a purely spherical configuration, the valence nucleons are solely neutrons, and the spin $g$-factor of neutrons is negative. It was assumed in [59] that the magnetic dipole moment operator has the form $\hat{M}1 = g_R(\beta)\mathbf{I}$, where $\mathbf{I}$ is the nucleus angular momentum operator, and also that $g_R(\beta)$ is equal to $-0.26$ at the spherical minimum and $Z/A$ at the deformed minimum, i.e., it changes sign inside the barrier separating the two minima.

## 7. Phase transitions in molecular-type rotational bands

Let us consider examples of second-order phase transitions in nuclei associated with octupole deformation. They are phase transitions in rotational bands that contain states of both parities; just such rotational bands are encountered in asymmetric two-atomic molecules. In fact, these are phase transitions from states in which the nucleus is not octupole-deformed to states with octupole deformation, occurring as the moment of rotation increases. The moment of rotation of the nucleus is a control parameter in this case. We see in what follows that the octupole deformation of the nucleus stabilizes as the moment of rotation increases.

In the discussion that follows, we assume that the main role in describing rotational bands of different parities is played by the octupole degree of freedom of the nucleus, which preserves the axial symmetry, i.e., $\beta_{30}$. The dynamical variable $\beta_{30}$ is similar to the $\beta$ variable introduced in Section 3,

but, in contrast to the latter, which describes quadrupole deformation of the nucleus, $\beta_{30}$ describes its octupole deformation. The $\beta$ variable in Section 3 could have been denoted as $\beta_{20}$. Nonzero values in the second subscript imply deviations from axial symmetry. Other octupole dynamical variables, which do not preserve the axial symmetry of the nucleus's shape, $\beta_{31}$, $\beta_{32}$, and $\beta_{33}$, also manifest themselves in excitations of the nucleus, but the corresponding states have higher excitation energies.

Let us comment on the spectrum of low-lying excited states of even–even deformed nuclei that have negative-parity states at moderate excitation energies. The lowest excited states of such nuclei are rotational bands, which in the vicinity of the ground state include positive-parity states with even moments of rotation, i.e., $0^+$, $2^+$, $4^+$, $6^+$, and so on. At higher excitation energies, negative-parity states appear, having odd moments of rotation: $1^-$, $3^-$, $5^-$, and so on. At moderate moments of rotation of the nucleus, negative-parity states are shifted up in energy by several hundred keV with respect to positive-parity states with similar angular momentum values, but as the angular momentum increases, this shift decreases, and a molecular-type rotational band is formed with the sequence of states $I^+$, $(I+1)^-$, $(I+2)^+$, and so on. The formation of such a rotational band is a consequence of the stabilization of the octupole deformation of the nucleus. Negative- and positive-parity states are associated with strong E1 transitions, considerably exceeding one-particle estimates in magnitude, which testifies to the similarity of the microscopic structure of such states. This problem is discussed in more detail in what follows.

Restricting ourself to only one dynamical variable, $\beta_{30}$, we start with the Hamiltonian [62, 63]

$$H_I = -\frac{\hbar^2}{2B}\frac{\mathrm{d}^2}{\mathrm{d}\beta_{30}^2} + V_I(\beta_{30})\,. \tag{30}$$

The subscript $I$ on the potential means that the shape of the potential depends on the moment of rotation. This is related to the fact that the potential $V_I(\beta_{30})$ also includes the energy of rotation. We also assume that the quadrupole deformation of the nucleus is fixed, i.e., is not a dynamical variable. Therefore, our analysis applies only to nuclei with a static quadrupole deformation, namely, to rare-earth and actinide nuclei. We do not assume any specific shape of the potential $V_I(\beta_{30})$, but use a procedure from supersymmetric quantum mechanics that allows determining the shape of the potential based on the expression for the wave function of the ground state. The following ansatz for the wave function of the lowest state for a given $I$ captures all the necessary features of the phenomenon under discussion:

$$\Psi_I(\beta_{30}) \sim \left\{\exp\left[-\frac{1}{2}\,s_3^2(I)\left(\frac{\beta_{30}}{\beta_{\mathrm{m}}(I)}-1\right)^2\right] + \exp\left[-\frac{1}{2}\,s_3^2(I)\left(\frac{\beta_{30}}{\beta_{\mathrm{m}}(I)}+1\right)^2\right]\right\}. \tag{31}$$

Wave function (31) is a sum of two Gaussians with maxima at $\beta_{30} = \pm\beta_{\mathrm{m}}(I)$. Because the change of sign of $\beta_{30}$ simply implies spatial reflection of the coordinate system and is not related to a change in the state of the nucleus, Hamiltonian (30) is invariant under the transformation $\beta_{30} \to -\beta_{30}$, and the wave function has a definite parity with respect to this transformation. Formally, the Schrödinger equation with the potential $V_I$ has an entire family of solutions with both parities for each value of $I$. But as follows from the symmetry properties of the wave function in the laboratory coordinate system [17], the lowest-energy rotational band of variable parity has only one state for a given $I$, whose parity is $(-1)^I$. In other words, this is a negative-parity state for an odd $I$. But among the eigensolutions of the Schrödinger equation with the potential $V_I$ in (30), the negative-parity solution is not the lowest but the first excited state. The corresponding excitation energy characterizes the experimentally observed parity shift in energies of the rotational band states based on the ground state.

The ansatz proposed in (31) allows describing both states of the nucleus without octupole deformation and octupole-deformed states. In the first case, $\beta_{\mathrm{m}}$ is close to zero and small compared with $s_3(I)$, and wave function (31) has only one maximum at $\beta_{30} = 0$. This implies that the most probable shape of the nucleus is the shape without octupole deformation. For $\beta_{\mathrm{m}}(I) \gg s_3(I)$, the maximum of the wave function shifts into the octupole deformation domain. As regards the $s_3(I)$ parameter, it follows from expression (31) that $s_3(I)$ characterizes the softness of the nucleus with respect to the octupole deformation. As $s_3(I) \to \infty$, the wave function acquires a sharp maximum at $\beta_{30} = \pm\beta_{\mathrm{m}}(I)$. As $s_3(I) \to 0$, the wave function is spread over a large domain of values of $\beta_{30}$.

We substitute wave function (31) in the Schrödinger equation with Hamiltonian (30). This yields the following relation for the potential $V_I(\beta_{30})$:

$$V_I(\beta_{30}) = \frac{\hbar^2}{2B}\,\Psi_I^{-1}(\beta_{30})\,\frac{\mathrm{d}^2\Psi_I(\beta_{30})}{\mathrm{d}\beta_{30}^2} + E_I^*\,, \tag{32}$$

where, for even $I$, $E_I^*$ coincides with the experimental excitation energy of the lowest state of the nucleus for a given $I$. For odd values of the moment of rotation, $E_I^*$ is determined by interpolation between experimental energies of neighboring states with even moments of rotation, i.e., between $E_{I-1}^*$ and $E_{I+1}^*$. This procedure is underlain by the fact that odd-$I$ states have negative parity and are shifted upward in energy relative to positive-parity states. At the same time, excitation energies of even-$I$ states are smooth functions of the moment of rotation. We assume that the derivatives $E_I^*$ are also smooth functions of $I$.

Substituting the expression for $\Psi_I$ from Eqn (31) into (32), we express the potential $V_I$ as

$$V_I(\beta_{30}) = \frac{\hbar\omega}{2}\left[-1 + s_3^2(I)\left(1+\frac{\beta_{30}^2}{\beta_{\mathrm{m}}^2(I)}\right) - 2s_3^2(I)\,\frac{\beta_{30}}{\beta_{\mathrm{m}}(I)} \times \frac{\exp\left(s_3^2(I)\beta_{30}/\beta_{\mathrm{m}}(I)\right) - \exp\left(-s_3^2(I)\beta_{30}/\beta_{\mathrm{m}}(I)\right)}{\exp\left(s_3^2(I)\beta_{30}/\beta_{\mathrm{m}}(I)\right) + \exp\left(-s_3^2(I)\beta_{30}/\beta_{\mathrm{m}}(I)\right)}\right] + E_I^*\,, \tag{33}$$

whence we see that the form of the potential is entirely determined by the parameter $s_3(I)$. An analysis of experimental data on state energies in variable-parity rotational bands has shown in [64] that $s_3(I)$ is described with good accuracy by a linear function of the moment of rotation,

$$s_3(I) = c_0 + c_1 I\,, \tag{34}$$

where constants $c_0$ and $c_1$ are to be determined for each nucleus from experimental data.

In Fig. 8, we show the results of a calculation based on experimental data on the $^{240}$Pu potential $V_I(\beta_{30})$ for $I = 2$,

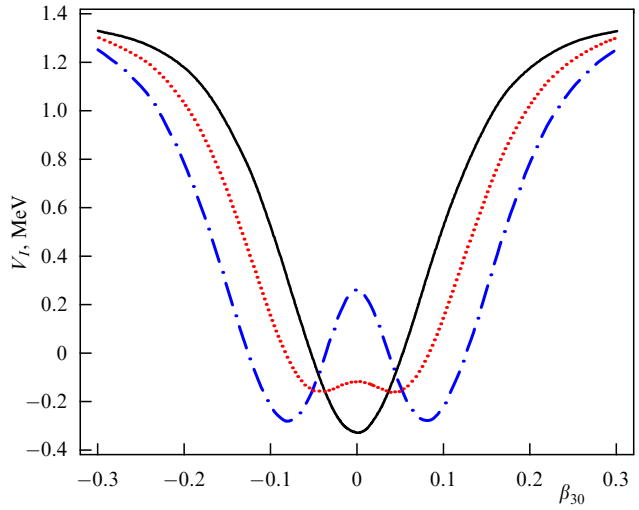


**Figure 8.** Collective potential $V_I(\beta_{30})$ for the $^{240}$Pu nucleus. The potential is calculated at the angular momentum values $I = 2$ (solid line), $I = 12$ (dotted line), and $I = 22$ (dashed-dotted line).

12, 22 [65]. The $^{240}$Pu nucleus was chosen, because there is more available experimental information on it than on other nuclei with known rotational bands of variable parity. We see from Fig. 8 that, at $I = 2$, the potential is close in shape to the harmonic oscillator potential near the $\beta_{30} = 0$ minimum. At $I = 22$, the potential has two minima, which suggests that the nucleus has an octupole-deformed shape. At $I = 12$, the potential takes a form characteristic of the transitional domain from the octupole-nondeformed to octupole-deformed shapes. Although the minimum of the potential at $I = 12$ is localized at $\beta_{30} = 0$, the amplitude of oscillations about the minimum is high. Therefore, in rotational bands containing states of both parities, a phase transition occurs as the moment of rotation increases.

In our case, the role of free energy in Landau's theory [47] is played by the value of $V_I$ at the minimum, $\beta_{30}$ is the order parameter, and the moment of rotation $I$ is the control parameter. The position of the minimum of the potential is defined by the condition

$$\left.\frac{\mathrm{d}V_I(\beta_{30})}{\mathrm{d}\beta_{30}}\right|_{\beta_{30}=(\beta_{30})_{\min}} = \hbar\omega\, s_3^2(I)\,\frac{(\beta_{30})_{\min}}{\beta_{\mathrm{m}}^2(I)} \times\left(1-\frac{(\beta_{30})_{\min}}{\beta_{\mathrm{m}}(I)}\tanh\left[s_3^2(I)\frac{(\beta_{30})_{\min}}{\beta_{\mathrm{m}}(I)}\right] -\frac{s_3^2(I)}{\cosh^2\left[s_3^2(I)(\beta_{30})_{\min}/\beta_{\mathrm{m}}(I)\right]}\right)=0\,. \tag{35}$$

One of the solutions of this equation is trivial: $(\beta_{30})_{\min} = 0$, which occurs if $s_3(I) < 1/\sqrt{2}$, when the second derivative of $V_I(\beta_{30})$ with respect to $\beta_{30}$ at the point of the minimum is positive. If $s_3(I) > 1/\sqrt{2}$, the potential attains a maximum at the point $\beta_{30} = 0$, and the minimum smoothly shifts toward nonzero values of $\beta_{30}$. The value at the minimum is the root of the equation

$$1-\frac{(\beta_{30})_{\min}}{\beta_{\mathrm{m}}(I)}\tanh\left[s_3^2(I)\frac{(\beta_{30})_{\min}}{\beta_{\mathrm{m}}(I)}\right] -\frac{s_3^2(I)}{\cosh^2\left[s_3^2(I)(\beta_{30})_{\min}/\beta_{\mathrm{m}}(I)\right]}=0\,. \tag{36}$$

If $s_3(I)$ is greater than but close to $1/\sqrt{2}$, the root of Eqn (36) can be approximately expressed as

$$(\beta_{30})_{\min} = \beta_{\mathrm{m}}(I)\sqrt{\frac{3}{2s_3^6(I)}\left(s_3^2(I)-\frac{1}{2}\right)}\,. \tag{37}$$

We next find the value of the potential at the minimum. If $s_3(I) < 1/\sqrt{2}$, then $(\beta_{30})_{\min} = 0$ and

$$V_I\big((\beta_{30})_{\min}\big) = \frac{1}{2}\,\frac{\hbar^2 s_3^2(I)}{B\beta_{\mathrm{m}}^2(I)}\big(-1+s_3^2(I)\big)+E_I^*\,. \tag{38}$$

If $s_3(I) > 1/\sqrt{2}$ but is close to $1/\sqrt{2}$, then

$$V_I\big((\beta_{30})_{\min}\big) \approx \frac{\hbar^2 s_3^2(I)}{B\beta_{\mathrm{m}}^2(I)} \times\left[-1+s_3^2(I)-\frac{3}{s_3^4(I)}\left(s_3^2(I)-\frac{1}{2}\right)^2\right]+E_I^*\,. \tag{39}$$

In expressions (38) and (39), higher-order terms in $(s_3^2(I) - 1/2)^2$ are omitted. Comparing (38) and (39), we see that $V_I((\beta_{30})_{\min})$ is a continuous function of $I$ at $s_3(I) = 1/\sqrt{2}$. The first derivatives of expressions (38) and (39) with respect to $I$ also coincide at $s_3 = 1/\sqrt{2}$. But the second derivatives undergo a discontinuity at $s_3(I) = 1/\sqrt{2}$. In differentiating, we used the fact that $s_3(I)$ is a linear function of $I$. Thus, in this case, we have a second-order phase transition.

Because the value $s_3(I) = 1/\sqrt{2}$ is critical for the phase transition under consideration, the critical value of the moment of rotation $I_{\mathrm{crit}}$ is determined in accordance with (34) by the relation

$$c_0 + c_1 I_{\mathrm{crit}} = \frac{1}{\sqrt{2}}\,. \tag{40}$$

The expression for $(\beta_{30})_{\min}$ can then be represented in the form

$$(\beta_{30})_{\min}(I) = \beta_{\mathrm{m}}(I_{\mathrm{crit}})\big[12\sqrt{2}\,c_1(I-I_{\mathrm{crit}})\big]^{1/2}\,. \tag{41}$$

Relation (41) is valid near the critical point. It follows from (41) that the critical exponent, i.e., the quantity describing the behavior of different characteristics of the system in a close neighborhood of the phase transition point, is equal to 1/2. The exact $(\beta_{30})_{\min}$ dependence can be obtained numerically from (36). The exact result for $^{240}$Pu is shown in Fig. 9 together with the approximate result (41).

The values of $I_{\mathrm{crit}}$ determined for $^{232}$Th, $^{238}$U, and $^{240}$Pu are as follows: 14.6 for $^{232}$Th, 12.7 for $^{238}$U, and 12.1 for $^{240}$Pu. Because our treatment of the phase transition is semiclassical, it is unsurprising that Eqn (36) yields noninteger values for $I_{\mathrm{crit}}$.

We have thus shown that, as the moment of rotation increases, a second-order phase transition from octupole-nondeformed to octupole-deformed states occurs in rotational bands comprising states of both parities.

To characterize a nucleus, it is not enough to know only the equilibrium value of the octupole deformation. It is also important that the magnitude of fluctuations of the deformation parameter about the equilibrium value be known. If a nucleus is octupole-deformed, then the octupole deformation potential energy has two physically equivalent minima, localized at positive and negative values of $\beta_{30}$ and separated

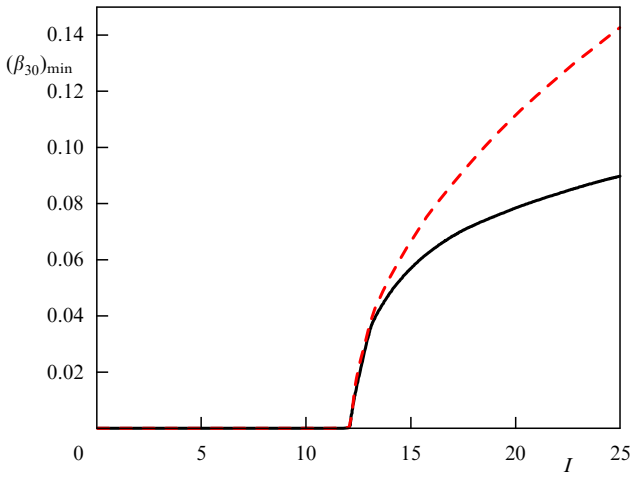


**Figure 9.** Dependence of $(\beta_{30})_{\min}$ on angular momentum $I$ for the $^{240}$Pu nucleus. The dashed line corresponds to the approximate dependence in Eqn (41). The solid line shows the exact result.

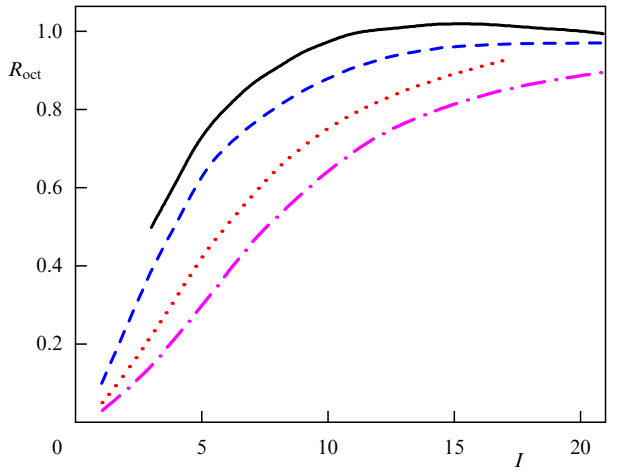


**Figure 10.** $R_{\text{oct}}$ as a function of angular momentum $I$. The solid line corresponds to $^{150}$Sm, the dotted line, to $^{152}$Sm, the dashed line, to $^{152}$Gd, and the dashed-dotted line, to $^{156}$Gd.

by a barrier. The probability of transmission through the barrier determines the shift in negative-parity energy levels with respect to positive-parity levels with close values of the angular momentum. The same probability also determines the amplitude of fluctuations. To characterize the amplitude of fluctuations, it is convenient to introduce a dimensionless quantity $R_{\text{oct}}$, the ratio of two energies, the energy that a state with angular momentum $I$ would have in the case of stabilization of the octupole deformation to the experimental energy of that state:

$$R_{\text{oct}}(I) = \frac{E_{\text{interpol}}(I)}{E_{\text{exp}}(I)} \,. \tag{42}$$

The energies $E_{\text{interpol}}(I)$ can be determined by interpolating between the energies of positive-parity states with moments of rotation $I-1$ and $I+1$. The dependence of $R_{\text{oct}}$ on $I$ for various nuclei is shown in Fig. 10, whence we see that, at small values of $I$, $R_{\text{oct}}$ is close to zero. This is caused by the high probability of transmission through the barrier. As $I$ increases, $R_{\text{oct}}$ increases, tending asymptotically to unity. This suggests that, at large $I$, positive- and negative-parity states form a single band of states with a similar microscopic structure. The dependence of $R_{\text{oct}}$ on the moment of rotation shown in Fig. 10 can be approximated with good accuracy by an exponential, similarly to the dependence of the relaxation of dielectric polarization in Debye's theory [66].

## 8. Superdeformed and hyperdeformed states

Another, and quite conspicuous, example of the coexistence of different shapes of a nucleus at different excitation energies is given by superdeformed states, whose deformation corresponds to the shape of an ellipsoid with the semiaxis ratio 2:1. Such states have already been known for more that 40 years, starting with the discovery of a fission isomer in Dubna [67]. But the most intense investigations of superdeformed states began in the late 1980s [68] due to their manifestation as higher-spin yrast states of rotational bands, i.e., the lowest-energy states among states with a given moment of rotation, with very high moments of inertia. For a long time, it had been impossible to experimentally find all the states of such bands with $I$ up to $I^{\pi} = 0^{+}$ in even–even nuclei, which did not allow determining absolute values of excitation energies and angular momenta of these states. The reason was that, at moderate angular momenta, the superdeformed states are in the domain of excitation energies with a high density of states that have the same angular momentum but a different structure. It is because of the high density of such states that superdeformed states, starting with some values of the angular momentum, undergo transitions, with the emission of gamma quanta, into states of a different structure rather than into superdeformed states with lower angular momenta. Later, the absolute values of superdeformed state energies were determined in the domain of nuclei with $A \sim 50$ [69–71].

The stability of superdeformed states is a consequence of shell effects, which are especially pronounced under certain relations between the deformation parameters of the mean field of the nucleus. For example, superdeformation is stabilized if the mean field of the nucleus can be approximated by a deformed oscillatory potential such that the ratios of frequencies corresponding to the different semiaxes are rational numbers [17].

A typical shape of the potential energy of deformation of a nucleus whose excitation spectrum contains a superdeformed rotational band is shown in Fig. 11. We see that, besides the minimum at which the ground state of the nucleus is localized, the potential has another minimum located at a higher deformation and higher energy, with the superdeformed band states localized there. As the angular momentum increases, due to a much larger moment of inertia, which is approximately proportional to the deformation squared, superdeformed states become lowest in energy among the states of the nucleus with the given angular momentum. As a result, in collisions with other heavy nuclei, when the nucleus is imparted a sufficiently large angular momentum, just the superdeformed states are observed.

In Fig. 11, we can see yet another minimum, which initially appears in calculations of the potential energy of deformation of the nuclei. It corresponds to hyperdeformed states, i.e., states of the nucleus with the deformation significantly exceeding $\beta = 0.6$. Hyperdeformed states are known in light nuclei. A classic example is provided by hyperdeformed states of $^{12}$C, based on $0^{+}_{2}$ states with the

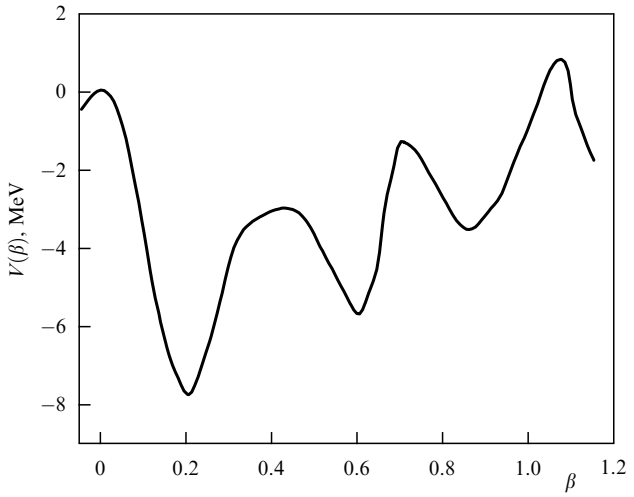


**Figure 11.** Typical shape of the quadrupole deformation potential energies of the nucleus with a superdeformed rotational band in the spectrum.

excitation energy 7.65 MeV. The shape of $^{12}$C in that state is represented as a linear chain of three alpha particles. Calculations predict that hyperdeformed states also exist in heavy nuclei. They are expected to become yrast states at moments of rotation of about $80\hbar$. Hyperdeformed states that are symmetric and nonsymmetric under spatial reflection are expected in Hg and Pb at excitation energies of the order of 6–8 MeV.

An example of a lighter nucleus with a superdeformed band and a distinct E2 transition into the ground-state band is provided by $^{60}$Zn. Interestingly, in nuclei with $A \sim 60$ and in lighter nuclei, superdeformation is closely related to the formation of a cluster structure.

Typical examples of clusterization in light nuclei are well known: $^{16}$O and $^{20}$Ne, in which the structures $^{12}\mathrm{C} + \alpha$ and $^{16}\mathrm{O} + \alpha$ are especially stable [72–74]. Interestingly, the cluster structure in $^{20}$Ne is realized in the rotational band of the ground state, whereas, in $^{16}$O, the cluster structure is associated with a rotational band constructed in the excited state with the excitation energy of 6.06 MeV. In papers [74, 75], clusterization is associated with the excited deformed rotational band in $^{40}$Ca and the ground-state band in $^{44}$Ti. In pairs of nuclei $^{16}\mathrm{O}-^{20}$Ne and $^{40}\mathrm{Ca}-^{44}$Ti, one of the partners is a doubly magic nucleus and the other is a doubly magic nucleus plus an alpha particle. The next pair of this type is given by $^{56}$Ni and $^{60}$Zn. It is known that in $^{56}$Ni a deformed rotational band based on an excited state exists at $I$ values up to $I^{\pi} = 12^{+}$. In $^{60}$Zn, the α-decay threshold exceeds the ground-state energy by only 2.7 MeV. Therefore, it is quite probable that the wave functions of the ground-state band have a more extensive α-cluster component. However, a superdeformed band is also known in $^{60}$Zn [69], in which only E2 transitions between the band states are observed for $I > 12$. However, in the range $I = 8-12$, E2 transitions from superdeformed band states are only possible into the ground-band states. The situation in $^{60}$Zn can therefore be characterized as the coexistence of different shapes of the nucleus, and the phase transition from one shape to another occurs as the excitation energy increases.

The moment of inertia of the superdeformed band of $^{60}$Zn, which depends on the angular momentum, takes values in the range of $(692-750)m$ fm$^2$, where $m$ is the nucleon mass. These values of the moment of inertia are close to the rigid-body moment of inertia of the cluster configuration $^{52}\mathrm{Fe} + {}^{8}\mathrm{Be}$, which is equal to $750m$ fm$^2$. We note that the thresholds of the $^{60}$Zn decay into $^{52}\mathrm{Fe} + {}^{8}\mathrm{Be}$ (10.8 MeV) and into $^{48}\mathrm{Cr} + {}^{12}\mathrm{C}$ (11.2 MeV) are close to the extrapolated value of the $0^{+}$-state energy (the base of the superdeformed band), 7.5 MeV.

It is therefore entirely possible that two families of states are realized in $^{60}$Zn. The first includes all states of the ground band with the cluster configuration $^{56}\mathrm{Ni} + \alpha$ as the main component, and the second includes states of the superdeformed band, whose main component is the cluster configuration $^{52}\mathrm{Fe} + {}^{8}\mathrm{Be}$ (or $\alpha + {}^{52}\mathrm{Fe} + \alpha$). We also note that the experimental value of the quadrupole moment of $^{60}$Zn, extracted from the values of the probabilities of E2 transitions at $I = 12-22$, is $(2.75 \pm 0.45)e$ bn. For the cluster configuration $^{52}\mathrm{Fe} + {}^{8}\mathrm{Be}$, depending on the accepted intercluster distance (0 or 0.5 fm), we obtain $(2.96-3.43)e$ bn. Thus, the cluster interpretation of the structure of the $^{60}$Zn superdeformed band is entirely justified.

Nuclear systems that have a cluster structure and consist of one heavy fragment with mass $A_1$ and one light fragment with mass $A_2$ belong to the class of double nuclear systems. In describing their shapes, it is convenient to use not the multipole expansions of the surface shape but the following two variables: the mass asymmetry $\eta = (A_1 - A_2)/(A_1 + A_2)$ and the distance $R$ between the fragment centers [76]. In strongly asymmetric double nuclear systems, the frequency of $R$ oscillations is much greater than the frequency of $\eta$ oscillations, and therefore in averaging over the oscillations we can set $R = R_{\mathrm{m}}(\eta)$, where $R_{\mathrm{m}}(\eta)$ is the distance between fragments at the minimum of the interaction potential. As a result, the problem reduces to describing the system with one dynamical variable $\eta$ and the Hamiltonian

$$H = -\frac{\hbar^2}{2}\frac{\mathrm{d}}{\mathrm{d}\eta}\frac{1}{B(\eta)}\frac{\mathrm{d}}{\mathrm{d}\eta} + U(\eta, I)\,, \tag{43}$$

where $U(\eta, I)$ is the potential energy and $B(\eta)$ is the coefficient of inertia. Eigenfunctions of Hamiltonian (43) are characterized by a definite parity under the transformation $\eta \to -\eta$, which is actually the spatial reflection. For double nuclear systems, the potential $U(\eta, I)$ has the form

$$U(\eta, I) = B_1 + B_2 - B_{12} + V_{\mathrm{C}} + V_{\mathrm{n}} + V_{\mathrm{rot}}\,, \tag{44}$$

where $B_1$ and $B_2$ are experimental values of the binding energy of the fragments, $B_{12}$ is the binding energy of a mononucleus with $A = A_1 + A_2$, $V_{\mathrm{C}}$ is the Coulomb potential, $V_{\mathrm{n}}$ is the nuclear potential of interaction of the fragments, and $V_{\mathrm{rot}}$ is the rotation energy of the double nuclear system. Calculations show that the $^{60}$Zn configuration with a light fragment, an α particle, has a potential energy 4.5 MeV less than the potential energy of the mononucleus. The next important minima of the potential, corresponding to configurations with the light fragments $^{8}$Be and $^{12}$C, are respectively higher than the mononucleus potential by 5.1 and 9.0 MeV (Fig. 12).

In Fig. 13, we show the distribution in $x$ ($x = \eta + 1$ if $\eta \leqslant 0$ and $x = \eta - 1$ if $\eta \geqslant 0$) of the squared wave functions of states with $I = 8$ from the ground and superdeformed bands. We see that the wave functions of states from different bands are clearly separated, but the overlap of the wave function tails is already sufficient for the superdeformed-band state to decay primarily into the ground band. At higher values of $I$,

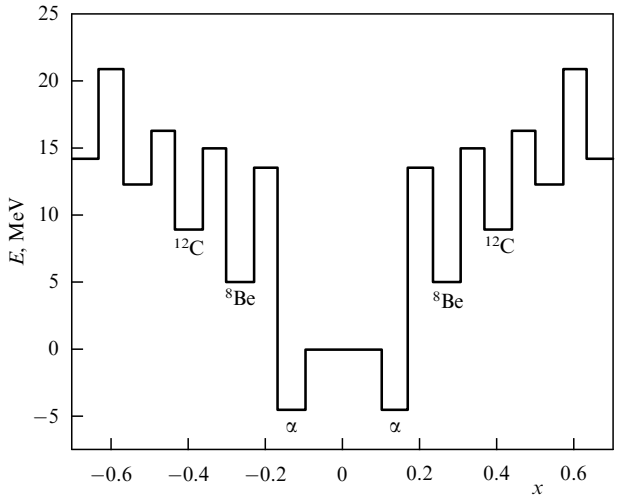


**Figure 12.** Potential energy of $^{60}$Zn as a function of the mass asymmetry parameter $x$.

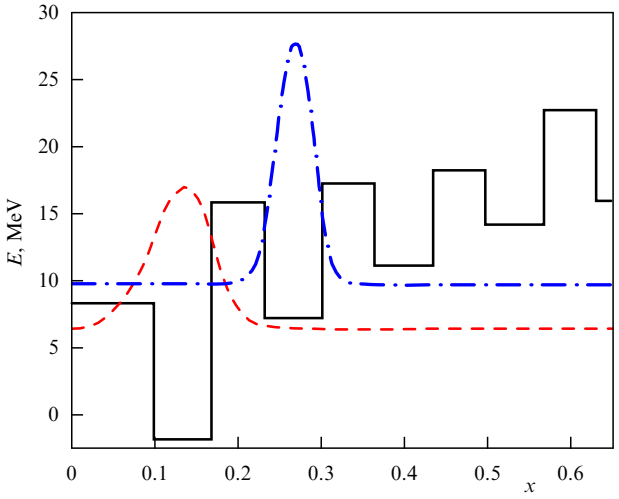


**Figure 13.** Distribution of squared wave functions of the ground (dashed line) and superdeformed (dashed-dotted line) states with $I = 8$ with respect to the mass asymmetry variable $x$; solid line shows the potential energy.

the separation of the wave functions becomes more pronounced.

## 9. Phase transitions and pair correlations in nuclei

The concept worked out for describing pair correlations of electrons in relation to superconductivity found immediate application in nuclear physics [77, 78] and played a key role in explaining the spectra of excited states of even–even nuclei, the even–odd mass difference, the rotational moments of inertia, and many other effects in nuclear physics.

The collective model for the description of pair correlations has been constructed both similarly to the geometric collective model of the nucleus [79–82] and based on the microscopic model of pair correlations with the use of bosonic representations of bifermionic operators [83, 84]. In considering pair correlations of nucleons of the same type (protons or neutrons), the dynamical variables are usually chosen as the pair correlation strength $\Delta$ and the angle $\phi$ describing orientation in the gauge space and canonically conjugate to the number-of-particles operator. The following Hamiltonian was proposed for describing collective motion associated with pair correlations [80]:

$$H_{\text{pair}} = -\frac{\hbar^2}{2B}\frac{\partial^2}{\partial\Delta^2} - \frac{\hbar^2}{4}\left(\frac{1}{\Im B}\frac{\partial\Im}{\partial\Delta} - \frac{1}{\Delta^2}\frac{\partial B}{\partial\Delta}\right)\frac{\partial}{\partial\Delta} + \left(V(\Delta) + \frac{\hbar^2\hat{N}^2}{2\Im}\right). \quad (45)$$

Here, $\Im$ and $B$ are the respective coefficients of inertia for pair rotations and pair vibrations, and $N = A - A_0$ is the number of particles in nucleus $A$ with respect to the number of particles in the base nucleus $A_0$. The form of the potential $V(\Delta)$ depends on the nature of pair correlations in a chosen nucleus. In nuclei with a moderate number of particles (holes) in the unfilled shell, there are no static pair correlations, and fluctuations of the pair field generate a vibrational spectrum [79]. For example, pair vibrational states are realized in nuclei adjacent to the doubly magic $^{208}$Pb, albeit with a significant anharmonicity. In nuclei whose valence shell is approximately half-filled, static pair correlations appear, and the ground states of the neighboring nuclei differing by two nucleons of the same type form the so-called pair rotational band [79]. The role of the angular variable is then played by the angle $\phi$ canonically conjugate to the number-of-particles operator $\hat{N}$. In that case, similarly to the collective model of the nucleus, we can speak of spontaneous symmetry breaking.

In the vibration limit, the potential $V(\Delta)$ has a minimum at $\Delta = 0$ and can be approximated by a harmonic oscillator; we can therefore set $B = \text{const}$ and $\Im = 4B\Delta^2$ [80]. Solving the Schrödinger equation with Hamiltonian (45) leads in this limit to an equidistant spectrum of pair excitations: $E \sim |A - A_0|$. The transition to static pair correlations is associated with a shift of the potential minimum to a nonzero value $\Delta = \Delta_0$. Assuming the potential to be more rigid at the minimum, we obtain a parabolic dependence of the energy of pair excitations on the number of particles: $E \sim (A - A_0)^2$. This dependence of the energy of ground states on the number of neutrons is observed in isotopes of Sn if $^{114}$Sn is taken as the base nucleus.

To describe the transition from the vibrational limit to static pair correlations, it was proposed in [85] to use an infinite rectangular well as the potential $V(\Delta)$.

In Table 3, we list the energies of the lowest states for each value of $N$ expressed in terms of the energy of the $N = 2$ state. The results are given for the harmonic oscillator potential, for the potential corresponding to the limit of static pair correlations, and for an infinite rectangular well modeling the domain of the phase transition from the vibrational to

**Table 3.** Energies of the lowest states for each value of $N$, normalized to the energy of the $N = 2$ state.

| $N$ | Vibrational limit | Potential of infinite rectangular well | Limit of static pair correlations | Experimental data* |
|---|---|---|---|---|
| 0 | 0 | 0 | 0 | 0 |
| 2 | 1 | 1 | 1 | 1 |
| 4 | 2 | 2.31 | 4 | 2.29 |
| 6 | 3 | 3.92 | 9 | 3.77 |
| 8 | 4 | 5.82 | 16 | 5.46 |
| 10 | 5 | 7.99 | 25 | 7.36 |
| 12 | 6 | 10.44 | 36 | 9.46 |

* For Pb isotopes with fewer than 126 neutrons (from [56]).

rotational limit. In the last column in Table 3, we list experimental data for Pb isotopes with the number of neutrons fewer than the magic number 126. We see that these results are close to those obtained for the phase transition domain.

We have considered pair correlations between nucleons of the same type in the case of heavy nuclei in which protons and neutrons fill different shells and, therefore, their wave functions overlap only weakly, while the difference between single particle energies is large compared to the pair interaction constant. Another picture is observed in lighter nuclei with $N = Z$, where we must consider not only neutron–neutron and proton–proton but also neutron–proton pair correlations. Thus, in discussing these nuclei, we must introduce isospin into consideration. To date, there has been no explicit experimental indication of the presence of isoscalar pair correlations, and we therefore introduce a collective pair Hamiltonian that takes only the isovector pair correlations into account. Under the assumption that the coefficient of inertia is independent of the collective variables, this Hamiltonian is given by [82, 83]

$$H_{\text{pair}} = \frac{\hbar^2}{2B}\left\{-\frac{1}{\Delta^5}\frac{\partial}{\partial\Delta}\Delta^5\frac{\partial}{\partial\Delta} - \frac{1}{\Delta^2\sin(4\theta)}\frac{\partial}{\partial\theta}\sin(4\theta)\frac{\partial}{\partial\theta} + \frac{1}{\Delta^2}\left[\frac{\left(\hat{N}/2 + \hat{T}_3\sin(2\theta)\right)^2}{\cos^2(2\theta)} + \hat{T}_3^2 + \frac{\hat{T}_1^2}{\cos^2\theta} + \frac{\hat{T}_2^2}{\sin^2\theta}\right]\right\} + \frac{1}{2}c\Delta^2 + d\Delta^4\left[3 - \cos(4\theta)\right]. \quad (46)$$

Here, $\Delta$ determines the magnitude of pair correlations and $\theta$ determines their isospin structure. The operator $\hat{N}$ characterizes the number of particles relative to the number of particles of the base nucleus, and $\hat{T}_i$ is the component of the isospin operator.

A detailed analysis of experimental data on nuclei with $N = Z$ has shown [86] that the $^{56}$Ni and $^{100}$Sn nuclei can be taken as the basic ones. However, because of the effect of subshells in $^{28}$Si and $^{80}$Zr nuclei, only a few nuclei with $N = Z$ — those located in the vicinity of $^{56}$Ni and $^{100}$Sn — can be regarded as excited pair states. Calculations based on Hamiltonian (46) for states with $T = 0$ have shown that the spectra of the first excited states in this domain of the nuclei are nearly equidistant. Thus, experimental data on the energies of ground states of the nuclei under consideration give no indications of phase transitions from the nonsuperfluid to the superfluid state.

## 10. Alignment of the angular momentum of an odd nucleon as a phase transition in rotational bands of odd deformed nuclei

An important role in determining the properties of rotational bands of odd deformed nuclei is played by the coupling of the angular momentum of an odd nucleon to the angular momentum of the even–even core, i.e., the Coriolis coupling. At small values of the total angular momentum of the nucleus $I$, this coupling is weak, the projection of the angular momentum of an odd nucleon on the symmetry axis $K$ of the nucleus is a good quantum number, and its value is defined by the mean field of the nucleus and the order of filling single particle levels [17]. As the total angular momentum increases, it becomes energetically advantageous to align the angular momentum of the odd nucleon along the rotation axis of the core (the axis that is perpendicular to the symmetry axis of the nucleus), because the associated increase in the single particle energy is then compensated by a greater decrease in the rotation energy. As a result, $K$ ceases to be a good quantum number, and the wave function of the odd nucleon becomes a superposition of components characterized by different values of $K$ [7]. Thus, $K$ becomes a dynamical variable.

The values taken by $K$ are, of course, discrete, but if the range of $K$ is not small, i.e., the angular momentum of an odd nucleon is sufficiently large, then a semiclassical treatment of the problem becomes possible, in which $K$, as was proposed by Mottelson, is considered a continuous variable. Assuming for simplicity that the angular momentum of an odd nucleon can take only one value $j$ (for example, in the case of the so-called intruder state with the opposite parity: $h_{11/2}, i_{13/2}$), we obtain the Hamiltonian [87]

$$H = -\frac{\hbar^2}{2\Im}\sqrt{(I^2 - K^2)(j^2 - K^2)}\,\frac{\mathrm{d}^2}{\mathrm{d}K^2} + U(K), \quad (47)$$

where $U(K)$ is the potential energy as a function of $K$:

$$U(K) = \frac{\hbar^2}{2\Im}(I - j)^2\left(1 + \frac{K^2}{Ij}\right) + \sqrt{\Delta^2 + (\kappa K^2 - \lambda)^2}. \quad (48)$$

Here, $\Im$ is the moment of inertia of the core, $\Delta$ is the parameter characterizing the strength of pair correlations, $\lambda$ is the chemical potential, and $\kappa$ is the quadrupole coupling constant between the odd nucleon and the core.

The potential energy $U(K)$ contains contributions from both the rotation energy of the nucleus and the energy of the odd nucleon. The first term has a minimum at $K = 0$, which is due to the fact that the rotation energy is minimal in the case of perfect alignment of the angular momentum of the odd nucleon along the axis perpendicular to the symmetry axis of the nucleus. The second term is minimal at the value of $K$ that characterizes the one-particle level nearest to the Fermi surface. As a result, the minimum of the total potential energy is determined by competition between these two terms. If

$$\frac{\hbar^2}{2\Im}(I - j)^2 < \frac{\lambda\kappa Ij}{\sqrt{\lambda^2 + \Delta^2}}, \quad (49)$$

then $U(K)$ has a minimum at $K = \pm K_0$, where $K_0 \neq 0$. This solution is realized if the deformation of the nucleus is large or the total angular momentum $I$ is close to $j$. This is the case of a strong coupling of the odd nucleon to the deformation of the mean field of the nucleus. The wave function of the lowest state for a given $I$ can be represented as the sum of two Gaussians located symmetrically at positive and negative values of $K$. Due to the symmetry of the Hamiltonian under the change of sign of $K$, the wave functions must be symmetric or antisymmetric combinations of two Gaussians. Tunneling through the barrier shifts the state with a symmetric wave function downward in energy, and the state with a nonsymmetric wave function upward. As a result, the expression for the state energy takes the following skeleton form:

$$E(I) = A(I) - (-1)^{I-j}B(I), \quad (50)$$

where $A(I)$ and $B(I)$ are smooth functions of $I$. In the case under consideration, $B(I)$ is small compared with $A(I)$ and can be treated perturbatively. Equation (50) describes the

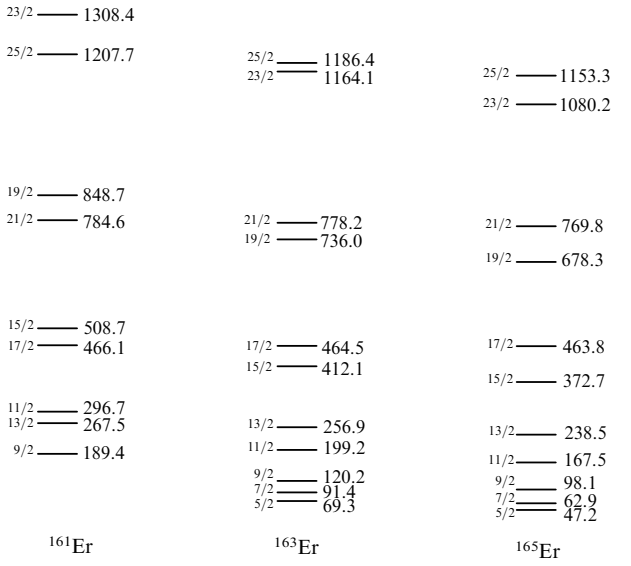


**Figure 14.** Experimental spectra of rotational states in Er isotopes illustrating the case of odd-nucleon angular momentum alignment along the rotation axis of the even–even core.

experimentally revealed effect of a staggering in the nucleus state energy as $I$ is stepped by one.

If condition (49) is not satisfied, the minimum of the potential is at $K = 0$, which corresponds to the perfect alignment of the angular momentum of the odd nucleon along the rotation axis of the nucleus, i.e., to the phase transition from one scheme of coupling the angular momentum of the odd nucleon and the angular momentum of the even–even core to another scheme. The potential can then be approximated by a harmonic oscillator centered at $K = 0$. The energies of states with different $I$ are still described by (50), but $B(I)$ is no longer small compared with $A(I)$.

In Fig. 14, we show the spectrum of excited states of Er isotopes [57], corresponding to the case of aligning the odd-nucleon angular momentum along the rotation axis of the even–even core at large values of the angular momentum. We see that, as the angular momentum increases, doublets start forming in the spectrum, comprising states with $\Delta I = 1$. The doublets appear because states with a symmetric wave function (9/2, 13/2, 17/2) are shifted downward in energy, and states with a nonsymmetric wave function (11/2, 15/2), upward.

## 11. Chirality in atomic nuclei

In rotating odd–odd nuclei that are not axially symmetric in shape, three angular momenta — the angular momentum of the even–even core and the angular momenta of the valence particle and hole — can determine the chiral geometry. These three pairwise perpendicular angular momenta constitute two physically equivalent coordinate systems — left-handed and right-handed — which are related by a chiral transformation that includes time reversal and rotation through 180° about one of the axes. When the chiral symmetry is broken in the internal coordinate system associated with the deformed core of the nucleus, two rotational bands with $\Delta I = 1$ appear in the laboratory system, each containing one of the members of the degenerate doublets with the same angular momenta (Fig. 15).

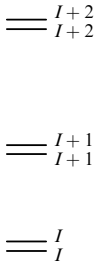


**Figure 15.** Example of the spectrum of degenerate rotational bands with $\Delta I = 1$ in the case where a potential barrier arises that separates the left-handed and right-handed configurations of angular momenta.

Static chirality is an effect well known in chemistry and biology as a geometric property of many molecules, especially biomolecules. In particle physics, chirality is a dynamical property dividing massless fermions into groups with parallel and antiparallel spins and momenta.

In the case of atomic nuclei, both chiral structures that pass one into another under time reversal and rotation through 180° about one of the principal axes of the core are realized as eigenstates of the nucleus, in contrast to the case of rotational bands, which we have seen include states of both parities. Therefore, associated with chirality in atomic nuclei is the appearance of two identical rotational bands with the same parity.

The occurrence of chirality in atomic nuclei was predicted in [88] in considering the coupling of angular momenta in nonaxial odd–odd nuclei. Since then, more than 20 such bands have been identified in the domains of the nuclide chart with $A \sim 100$, 130, and 190 [88–92]. The observed moderate difference in energies of states with the same angular momenta $I$ in rotational bands of chiral partners points to the existence of chiral vibrations from the right-handed (left-handed) configuration to the left-handed (right-handed) one [93, 94]. A decrease in energy splitting suggests that chiral vibrations transform into tunneling between well-stabilized chiral configurations (static chirality). This happens as the angular momentum $I$ of the nucleus increases. In calculations with the $^{135}$Nd nucleus [94], chirality attains the maximum staticity at $I = 39/2$, when both rotational partner bands come very close to one another in energy.

To describe the energy splitting of chiral doublets, we must go beyond the mean field approximation, to which the cranking model belongs, where the direction of the moment of rotation does not coincide in general with any of the principal axes of the nucleus [95]; a collective Hamiltonian must be constructed instead. The orientation of the rotation axis of the nucleus relative to the principal axes of the density distribution in a deformed nucleus is given by

$$\boldsymbol{\omega} = (\omega \sin\theta \cos\varphi, \omega \sin\theta \sin\varphi, \omega \cos\theta)\,, \tag{51}$$

where $\boldsymbol{\omega}$ is the angular velocity vector. The system of principal axes can be determined using the quadrupole moment of the density distribution $Q_{\rm m}$. In the coordinate system associated with the principal axes,

$$Q_1 = Q_{-1} = 0\,, \quad Q_2 = Q_{-2}\,. \tag{52}$$

In Ref. [96], an operator $\hat{\sigma}$ was introduced that characterizes the chiral degree of freedom of the nucleus:

$$\hat{\sigma} = \left(\hat{\mathbf{j}}_\pi \times \hat{\mathbf{j}}_\nu\right) \hat{\mathbf{R}} = |j_\pi|\,|j_\nu|\,|R|\,\sin\theta_{\rm PN} \sin\theta \sin\varphi\,, \tag{53}$$

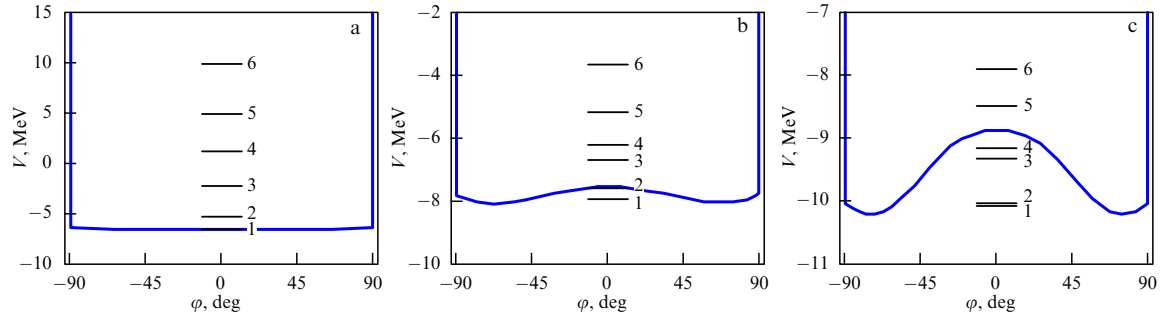


**Figure 16.** Evolution of the potential $V(\varphi)$ and the six lowest levels in the spectrum with an increase in the rotation frequency $\omega$ in nuclei with configurations involving left-handed and right-handed orientations of angular momenta of the odd nucleons and the even–even core: (a) $\hbar\omega = 0.25$ MeV, (b) $\hbar\omega = 0.35$ MeV, and (c) $\hbar\omega = 0.45$ MeV.

where $\hat{\mathbf{j}}_\pi$ is the angular momentum operator of the proton particle, $\hat{\mathbf{j}}_\nu$ is the angular momentum operator of the neutron hole, $\hat{\mathbf{R}}$ is the angular momentum operator of the even–even core, and $\theta_{\rm PN}$ is the angle between $\hat{\mathbf{j}}_\pi$ and $\hat{\mathbf{j}}_\nu$. The eigenvalues of $\hat{\sigma}$ have opposite signs for left-handed and right-handed systems. As defined in [88], the angle $\theta$ ranges in the interval $0 \leqslant \theta \leqslant \pi/2$, and the $\varphi$ angle, in the interval $-\pi/2 \leqslant \varphi \leqslant \pi/2$. Thus, $\varphi$ is a dynamical variable that describes the transition from the left-handed to the right-handed system. The collective Hamiltonian incorporating the chiral degree of freedom then becomes

$$\hat{H}_{\rm coll} = T_{\rm vib}(\varphi) + V(\varphi)\,, \tag{54}$$

or in the quantized form

$$\hat{H}_{\rm coll} = -\frac{\hbar^2}{2\sqrt{B(\varphi)}}\frac{\mathrm{d}}{\mathrm{d}\varphi}\sqrt{B(\varphi)}\,\frac{\mathrm{d}}{\mathrm{d}\varphi} + V(\varphi)\,. \tag{55}$$

Details of the calculation of the mass coefficient can be found in [97]. The volume element in this collective space is given by

$$\int \mathrm{d}\tau_{\rm coll} = \int \mathrm{d}\varphi\,\sqrt{B(\varphi)}\,, \tag{56}$$

and, hence, with collective measure (56), $\hat{H}_{\rm coll}$ is Hermitian. The potential $V(\varphi)$ can be calculated in the mean field approximation, given the magnitude and direction of the angular momentum of the nucleus [98]. The potential $V(\varphi)$ is symmetric with respect to $\varphi = 0$. This means that eigenfunctions of Hamiltonian (55) are characterized by a definite parity under the change of sign of $\varphi$.

As the rotation frequency increases, the minimum of the potential, which was first located at $\varphi = 0$, shifts toward nonzero values of $\varphi$. At small angular momenta, the potential $V(\varphi)$ can be approximated by a harmonic oscillator potential. At large angular momenta, $V(\varphi)$ acquires two symmetric minima. Accordingly, the barrier that separates them increases as the rotation frequency $\omega$ increases.

In Fig. 16, we show how the potential and the spectrum of excited states evolve [98] as the rotation frequency increases. Six eigenstates of the Hamiltonian that are lowest in energy are presented. We see that, as the angular momentum increases, the levels in three pairs (1st and 2nd, 3rd and 4th, and 5th and 6th) come closer to each other. As the angular momentum increases, the barrier in the potential grows in height and width, and therefore the tunneling probability decreases and the energy split of levels in the pairs tends to zero.

The wave function of the lowest-energy state is symmetric under the transformation $\varphi \to -\varphi$ and has no nodes. The wave function of the next-in-energy state is asymmetric. Among the states of the following doublets lower in energy is a state, there is one whose wave function is symmetric under $\varphi \to -\varphi$.

Both rotational bands, which are chiral partners, have been revealed in a number of nuclei. Examples are given by $^{134}$Pr and its isotones: $^{130}$Cs, $^{132}$La, and $^{134}$Pm [89].

## 12. Conclusions

Phase transitions in atomic nuclei, the coexistence of shapes revealed in various domains of the nuclide chart, are no longer a curiosity, as they used to be at the initial stage of investigations of the structure of nuclei. These phenomena can naturally be studied within collective models of the nucleus, containing a moderate number of degrees of freedom of the nucleus that are most important for describing phase transitions. At the same time, understanding the mechanism behind these phenomena requires an underlying microscopic approach, with its most important component being the concept of the mean field of the nucleus, its most prominent feature being shells and subshells in the spectrum of one-particle states.

All examples of phase transitions considered above, associated with different degrees of freedom of the nucleus and characterized by different control parameters, can in the simplest approximation be considered within a general scheme: one-dimensional or two-dimensional Schrödinger equations with a two-minimum potential. This allows revealing common features in different observable phenomena and drawing analogies with well-known phase transition phenomena in macrophysics.

This paper was supported by the Russian Foundation for Basic Research, grant no. 19-12-50172.

## References

1. Bohr A *Mat. Fys. Medd. Dan. Vid. Selsk.* **26** 14 (1952)
2. Davydov A S, Filippov G F *Sov. Phys. JETP* **8** 303 (1959); *Zh. Eksp. Teor. Fiz.* **35** 440 (1958)
3. Ring P, Schuck P *The Nuclear Many-Body Problem* (Berlin: Springer-Verlag, 2004)
4. Butler P A, Nazarewicz W *Rev. Mod. Phys.* **68** 349 (1996)
5. Bogolyubov N N *Dokl. Akad. Nauk SSSR* **119** 52 (1958)
6. Bohr A, Mottelson B R, Pines D *Phys. Rev.* **110** 936 (1958)
7. Stephens F S *Rev. Mod. Phys.* **47** 43 (1975)
8. Frauendorf S, Meng J *Nucl. Phys. A* **617** 131 (1997)

9. Morinaga H *Phys. Rev.* **101** 254 (1956)
10. Heyde K, Wood J L *Rev. Mod. Phys.* **83** 1467 (2011)
11. Poves A *J. Phys. G* **43** 024010 (2016)
12. Goeppert Mayer M, Jensen J H D *Elementary Theory of Nuclear Shell Structure* (New York: Wiley, 1955); Translated into Russian: *Elementarnaya Teoriya Yadernykh Obolochek* (Moscow: IL, 1958)
13. Reinhardt P-G, Otten E W *Nucl. Phys. A* **420** 173 (1984)
14. Bohr N *Nature* **137** 344 (1936)
15. Balian R, Bloch C *Ann. Physics* **60** 401 (1970)
16. Brack M et al. *Rev. Mod. Phys.* **44** 320 (1972)
17. Bohr A, Mottelson B R *Nuclear Structure* (New York: W.A. Benjamin, 1969); Translated into Russian: *Struktura Atomnogo Yadra* Vol. 2 (Moscow: Mir, 1977)
18. Federman P, Pittel S *Phys. Lett. B* **69** 385 (1977)
19. de-Shalit A, Goldhaber M *Phys. Rev.* **92** 1211 (1953)
20. Talmi I *Rev. Mod. Phys.* **34** 704 (1962)
21. Heyde K et al. *Phys. Lett. B* **155** 303 (1985)
22. Cohen B L, in *Proc. Intern. Symp. on Nuclear Structure, Dubna, 4–11 July, 1968* (Vienna: IAEA, 1968) p. 3
23. Otsuka T et al. *Phys. Rev. Lett.* **95** 232502 (2005)
24. Talmi I *Simple Models of Complex Nuclei* (Harwood, CA: Harwood Acad. Publ., 1993)
25. Belyaev S T *Kgl. Dan. Vid. Selsk. Mat.-Fys. Medd.* **31** 11 (1959)
26. Solov'ev V G *Sov. Phys. JETP* **8** 572 (1959); *Zh. Eksp. Teor. Fiz.* **35** 823 (1958)
27. Solov'ev V G *Sov. Phys. JETP* **9** 1331 (1959); *Zh. Eksp. Teor. Fiz.* **36** 1869 (1959)
28. Lane A *Nuclear Theory* (New York: W.A. Benjamin, 1964)
29. Bohr A, Mottelson B *Mat. Fys. Medd. Dan. Vid. Selsk.* **27** 16 (1953)
30. Elliott J P *Proc. R. Soc. Lond. A* **245** 128 (1956)
31. Elliott J P *Proc. R. Soc. Lond. A* **245** 562 (1958)
32. Iachello F, Arima A *The Interacting Boson Model* (Cambridge: Cambridge Univ. Press, 1987)
33. Janssen D, Jolos R V, Dönau F *Nucl. Phys. A* **224** 93 (1974)
34. Gamow G *Proc. R. Soc. Lond. A* **126** 632 (1930)
35. v. Weizsäcker C F *Z. Phys.* **96** 431 (1935)
36. Rowe D J, Wood J L *Fundamentals of Nuclear Models. Foundational Models* (Hackensack, NJ: World Scientific, 2010)
37. Wilets L, Jean M *Phys. Rev.* **102** 788 (1956)
38. Jolos R V, Dönau F, Janssen D *Theor. Math. Phys.* **20** 704 (1974); *Teor. Mat. Fiz.* **20** 112 (1974)
39. Soloviev V G *Theory of Complex Nuclei* (Oxford: Pergamon Press, 1976); Translated from Russian: *Teoriya Slozhnykh Yader* (Moscow: Nauka, 1971)
40. Bohr A, Mottelson B R *Phys. Scripta* **22** 468 (1980)
41. Ginocchio J N, Kirson M W *Phys. Rev. Lett.* **44** 1744 (1980)
42. Ginocchio J N, Kirson M W *Nucl. Phys. A* **350** 31 (1980)
43. Dieperink A E L, Scholten O, Iachello F *Phys. Rev. Lett.* **44** 1747 (1980)
44. Jolie J et al. *Phys. Rev. Lett.* **89** 182502 (2002)
45. Jolie J et al. *Phys. Rev. Lett.* **87** 162501 (2001)
46. Cejnar P, Jolie J, Casten R F *Rev. Mod. Phys.* **82** 2155 (2010)
47. Landau L D *Zh. Eksp. Teor. Fiz.* **7** 19 (1937); Landau L *Phys. Z. Sowjetunion* **11** 26 (1937); Landau L D *Zh. Eksp. Teor. Fiz.* **7** 627 (1937); Landau L *Phys. Z. Sowjetunion* **11** 545 (1937)
48. Jolos R V *Fiz. Elem. Chastits At. Yadra* **35** 407 (2004)
49. Casten R F *Nat. Phys.* **2** 811 (2006)
50. Fossion R *Rev. Mexicana Fisica S* **54** 42 (2008)
51. Iachello F *Phys. Rev. Lett.* **85** 3580 (2000)
52. Iachello F *Phys. Rev. Lett.* **87** 052502 (2001)
53. Jolos R V, von Brentano P *Phys. Rev. C* **80** 034308 (2009)
54. Casten R F, Zamfir N V *Phys. Rev. Lett.* **85** 3584 (2000)
55. García-Ramos J E, Heyde K *Phys. Rev. C* **100** 044315 (2019)
56. National Nuclear Data Center, https://www.nndc.bnl.gov/
57. Witt W et al. *Eur. Phys. J. A* **55** 79 (2019)
58. Kremer C et al. *Phys. Rev. Lett.* **117** 172503 (2016)
59. Sazonov D A et al. *Phys. Rev. C* **99** 031304(R) (2019)
60. Jolos R V, von Brentano P *Phys. Rev. C* **76** 024309 (2007)
61. Jolos R V, von Brentano P *Phys. Rev. C* **77** 064317 (2008)
62. Jolos R V, von Brentano P *Phys. Rev. C* **84** 024312 (2011)
63. Jolos R V, von Brentano P, Jolie J *Phys. Rev. C* **86** 024319 (2012)
64. Jolos R V, von Brentano P *Phys. Rev. C* **92** 044318 (2015)
65. Jolos R V, von Brentano P, Casten R F *Phys. Rev. C* **88** 034306 (2013)
66. Jolos R V et al. *Phys. Atom. Nucl.* **83** 550 (2020); *Yad. Fiz.* **83** 309 (2020)
67. Polikanov S M et al. *Sov. Phys. JETP* **15** 1016 (1962); *Zh. Eksp. Teor. Fiz.* **42** 1464 (1962)
68. Twin P J et al. *Phys. Rev. Lett.* **57** 811 (1986)
69. Svensson C E et al. *Phys. Rev. Lett.* **79** 1233 (1997)
70. Svensson C E et al. *Phys. Rev. Lett.* **82** 3400 (1999)
71. Rudolf D et al. *Phys. Rev. Lett.* **86** 1450 (2001)
72. Buck B, Dover C B, Vary J P *Phys. Rev. C* **11** 1803 (1975)
73. Michel F, Okhubo S, Reidermeister G *Prog. Theor. Phys. Suppl.* **132** 7 (1998)
74. Yamaya T et al. *Prog. Theor. Phys. Suppl.* **132** 73 (1998)
75. von Oertzen W, Freer M, Kanada-En'yo Y *Phys. Rep.* **432** 43 (2006)
76. Adamian G G et al. *Phys. Rev. C* **67** 054303 (2003)
77. Broglia R A, Zelevinsky V (Eds) *Fifty Years of Nuclear BCS*: *Pairing in Finite Systems* (Singapore: World Scientific, 2013)
78. Brink D, Broglia R A *Nuclear Superfluidity*: *Pairing in Finite Systems* (New York: Cambridge Univ. Press, 2005)
79. Bohr A, in *Proc. Intern. Symp. on Nuclear Structure, Dubna, 4–11 July, 1968* (Vienna: IAEA, 1968) p. 179
80. Bès D R et al. *Nucl. Phys. A* **143** 1 (1970)
81. Dussel G G, Perazzo R P J, Bès D R *Nucl. Phys. A* **183** 298 (1972)
82. Dussel G G et al. *Nucl. Phys. A* **175** 513 (1971)
83. Djolos R V et al. *Theor. Math. Phys.* **14** 51 (1973); *Teor. Mat. Fiz.* **14** 70 (1973)
84. Jolos R V, Kartavenko V G, Kolganova E A *Phys. Part. Nucl.* **49** 125 (2018); *Fiz. Elem. Chastits At. Yadra* **49** 229 (2018)
85. Clark R M et al. *Phys. Rev. Lett.* **96** 032501 (2006)
86. Nikoghosyan G, Kolganova E A, Sazonov D A, Jolos R V *Eur. Phys. J. A* **55** 189 (2019)
87. Jolos R V, Gelberg A *Phys. Lett. B* **317** 495 (1993)
88. Frauendorf S, Meng J *Z. Phys. A* **356** 263 (1996)
89. Starosta K et al. *Phys. Rev. Lett.* **86** 971 (2001)
90. Koike T et al. *Phys. Rev. C* **63** 061304(R) (2001)
91. Zhu S et al. *Phys. Rev. Lett.* **91** 132501 (2003)
92. Joshi P et al. *Phys. Lett. B* **595** 135 (2004)
93. Mukhopadhyay S et al. *Phys. Rev. Lett.* **99** 172501 (2007)
94. Qi B et al. *Phys. Lett. B* **675** 175 (2009)
95. Frauendorf S *Nucl. Phys. A* **557** 259 (1993)
96. Starosta K et al. *Nucl. Phys. A* **682** 375 (2001)
97. Rowe D J *Nuclear Collective Motion*: *Models and Theory* (London: Methuen, 1970)
98. Chen Q B et al. *Phys. Rev. C* **87** 024314 (2013)